Predicting Bond-Currents in Polybenzenoid Hydrocarbons with an Additivity Scheme

Author(s):
Paenurk, Eno; Feusi, Stefan; Gershoni-Poranne, Renana

Publication date:
2021

Permanent link:
https://doi.org/10.3929/ethz-b-000461276

Originally published in:
The Journal of Chemical Physics 154(2), https://doi.org/10.1063/5.0038292

The Journal of Chemical Physics

Predicting Bond-Currents in Polybenzenoid Hydrocarbons with an Additivity Scheme

Eno Paenurk, Stefan Feusi, and Renana Gershoni-Poranne

Laboratorium für Organische Chemie, ETH Zurich, Switzerland

renana.poranne@org.chem.ethz.ch

Abstract

We report on the construction and application of a new bond-current additivity scheme for polybenzenoid hydrocarbons. The method is based on identification of the smaller substructures contained in the system, up to tricyclic subunits. Thus, it enables the prediction of any *cata*-condensed unbranched polybenzenoid hydrocarbon, using a library consisting of only four building blocks. The predicted bond-currents can then be used to generate NICS values, the results of which validate previous observations of additivity with NICS-XY-Scans. The limitations of the method are probed, leading to clearly delineated and apparently constant error boundaries, which are independent of the molecular size. It is shown that there is a relationship between the accuracy of the predictions and the molecular structure and specific motifs that are especially challenging are identified. The results of the additivity method, combined with the transparent description of its strengths and weaknesses, ensure that this method can be used with well-defined reliability for characterization of polybenzenoid hydrocarbons. The resource-efficient and rapid nature of the method make it a promising tool for screening and molecular design.

Introduction

Aromatic systems are among the most prevalent compounds in nature and man-made materials. In particular, over the past few decades, polycyclic aromatic systems (PASs) have become the workhorse of organic electronics.[1,2] This is due to the molecular properties that characterize these systems: they are π-conjugated, which allows for conductance,[1,3] yet are relatively stable, as compared to other conjugated systems, e.g., polyenes;[4] they tend to pack closely,[5,6] which is important for charge mobility;[7] and they can be relatively easily modified through substitution with functional groups or annulation, which allows for tuning their electronic properties,[8–10] as well as other attributes, e.g., solubility.[11,12] The ability to tune their electronic properties is one of the greatest advantages of PASs as organic electronics because, in order to perform in such a capacity, the molecule must meet certain requirements. For example, a HOMO-LUMO

gap in a specific range and/or HOMO and LUMO levels that complement the work functions of the electrodes.[13–15]

The chemical community, and physical organic chemists in particular, have been fascinated by the electronic structure and reactivity of aromatic systems for over 150 years. With their additional importance as functional molecules and materials, this conceptual interest has taken on a practical aspect in the past few decades, as well. One of the different ways to identify and evaluate aromaticity is with magnetic criteria, which are described by the Ring-Current Model (RCM). The model was originally proposed, independently and essentially simultaneously by Pauling[16] and Lonsdale,[17] to explain the magnetic anisotropy observed in aromatic molecules. London[18] later merged this notion with Hückel's molecular orbital theory to afford a quantum mechanical treatment. Pople[19] and McWeeny[20] are credited with subsequent developments leading to the present version of the RCM (for further reading into the history of the RCM, see 21 and 22). In short, according to the RCM, placing an aromatic molecule into an external magnetic field perpendicular to the molecular plane induces a ring-current, which in turn induces a magnetic field. Various methods have been developed to qualitatively and/or quantitatively assess aromaticity via these different magnetic responses. One of the most common techniques in this domain is the Nucleus Independent Chemical Shift (NICS)[23–25] metric, which evaluates the strength of the induced magnetic current at a specified location. For PASs, an extension of the method, termed the NICS-XY-Scan,[26] is commonly used (we explain more about these two methods in Appendix A). NICS-XY-Scans have already been used to characterize organic semiconductors and to aid in the design of novel compounds,[27–30] by identifying and evaluating the aromatic nature of systems. Moreover, a few years ago, it was demonstrated that $NICS(r)_{\pi ZZ}$ is quantitatively correlated to the HOMO-LUMO gap and Ionization Potential.[31] This means that the NICS-XY-Scan can be used to also predict specific physical properties.

While the NICS-XY-Scan is a helpful tool, in some cases obtaining NICS values at an accurate level may require the same computational resources as simply calculating the properties of interest. A couple of years ago, we showed that NICS-XY-Scans can be generated with an additivity scheme (which is explained in detail in the appropriate section).[32,33] One of the main advantages of the additivity method is that it allows generation of NICS-XY-Scans for large and diverse PASs in far less time and using far fewer computational resources. Very recently, we automated the additivity method in a Python-based program, Predi-XY,[34] which further cuts down the computation time (by five orders of magnitude, with the hardware we tested) and the manual labor required to generate the scan. Thus, we can now obtain predicted NICS-XY-Scans for PASs at a substantially reduced computational cost and in a fraction of a second. By reducing the costs of time and resources so dramatically, Predi-XY has the potential to make the NICS-XY-Scan a much more

widely applicable tool for molecular design. Due to this, we believe a deeper look into the additive behavior at its base is warranted.

So far, we have tested the additivity scheme on various systems with eight different types of monocyclic subunits systems and containing up to ten rings, and have been very gratified to see that it performs well. Yet, we recognize that this apparent success is phenomenological and is not based on rigorous derivation. In other words: it seems to work, but does it reflect the true behavior of the system? This question is especially important given the general criticism of the NICS method. As an integrative method, NICS reduces the wealth of data in the vector field of the induced current density to a single scalar value or an array of values if a scan is performed.[35] Thus, though a recent investigation of 60 charged and neutral molecules showed that NICS-XY-Scans and current density agree in their description of the aromatic behavior,[36] could it be that the additivity implied by the NICS-XY-Scans is a result of the approximations inherent in this method? Could it be an accidental cancellation of effects that leads to an apparent additivity? Whether this is the case or not, how can this be determined? Our approach was to return to the original premise of the magnetic criterion of aromaticity, the RCM. NICS was developed as a tool to assess the induced magnetic field, which stems from the induced ring-currents. Thus, to verify the observation of additive behavior implied by NICS, we set out to determine whether the underlying property behaves in a similar manner, i.e., we set out to reproduce our NICS-based additivity with current density.

Herein, we report on the construction and benchmarking of a new additivity scheme, based on magnetically induced bond-current strengths (henceforth, referred to as "bond-current strengths" or BCS, for conciseness) as a model for the induced current density. This scheme demonstrates that the bond-currents in polybenzenoid hydrocarbons (PBHs) have the same additive behavior as their NICS-XY-Scans. Moreover, the molecular bond-currents generated by the new scheme can themselves be used as the basis for predicting NICS-XY-Scans. We also probe the limitations of the additivity method, highlight challenging cases, and delineate the error margins that can be expected. Overall, this work serves to corroborate the additive nature we previously reported on and to clearly define the accuracy of the method, the latter of which is key to responsible and meaningful use.

The NICS-XY-Scan Additivity Scheme (NAdd)

The main goals of this report are to investigate and discuss the issue of additivity of current density and its link to the apparent NICS additivity. Therefore, it is important to briefly explain the NICS-XY-Scan Additivity method (for conciseness, we shall refer to it from this point as the NAdd, and to NICS values obtained with this method as $NICS^{NAdd}$). For further details and examples, we refer the reader to the original publications introducing the method.[32,33] In the NAdd, we define two main components: building blocks

and combination rules. The building blocks are the monocyclic, bicyclic, and tricyclic subunits; for PBHs, these are benzene (**1_0**), naphthalene (**2_0**), anthracene (**3_0**), and phenanthrene (**3_1**). The combination rules are applied based on the sequence in which the individual subunits appear in the larger system. To clarify this, we show an example in Figure 1a. In our method, this PBH is seen as a superposition of all of the subunits it contains. The sequence of subunits is determined by "reading" the molecule; the direction of "reading" is arbitrary and does not change the results, other than reversing the direction of the final predicted scan. In Figure 1b we "read" the sample molecule from left to right (our conventional direction) and show that it contains five benzenes (green), four naphthalenes (pink), two phenanthrenes (light blue), and one anthracene (dark blue). Just as the subunits overlap in space, their NICS-XY-Scans should overlap in the additive calculation (Figure 1c, same color-coding), and therefore their NICS-XY-Scans also overlap (Figure 1d, same color-coding). To obtain the final prediction, all contributions are summed for each distance point (dashed gray curve in Figure 1d).

To avoid "double-" and "triple-counting", we use Bicyclic Corrections (BC) and Tricyclic Corrections (TC) in place of the explicit scans for these subunits. The BC is the difference between the explicitly calculated NICS-XY-Scan of the bicyclic system and the superimposed monocyclic subunits; the TC is the difference between the explicitly calculated NICS-XY-Scan of the tricyclic system and the superimposed monocyclic subunits and BCs. By using these terms, we are "correcting" each benzene ring with the change it undergoes when it becomes part of a naphthalene and then part of an anthracene/phenanthrene. The success of this approach is evident in the final predicted scan (the $NICS^{NAdd}$ curve, dashed gray), which shows remarkable agreement with the explicitly calculated scan for the pentacyclic system (black).

Figure 1. Example of the NAdd procedure. a) Scheme of sample pentacyclic PBH and the pathway of the scan through it. b) Color-coded identification of the building blocks contained in the sample molecule: monocyclic (green), bicyclic (pink), tricyclic (light blue—angular, dark blue—linear). c) Schematic illustration of the superposition of building blocks, color-coded as in (b). d) Plot of superimposed NICS-XY-Scans of the individual building blocks, color-coded as in (b); the sum of contributions (dashed gray) and the explicitly calculated NICS-XY-Scan (black). Double-bonds are omitted for clarity. Figure reproduced from Ref. [33].

An important conclusion from the NAdd is that the final scan, consisting of the $NICS^{NAdd}$ values, will be determined by the sequence of tricyclic subunits [linearly annulated (*L*) or angularly annulated (*A*)] that make up the molecule. To understand this, consider the isomers of pentacyclic PBHs shown in Figure 2. In our examples, "reading" the molecules left-to-right, **6_3** has the sequence *ALLA* and **6_13** and **6_14** both have the annulation sequence *ALAA*. The monocyclic and bicyclic subunits are identical for all three isomers (five benzenes, four naphthalenes); they differ only in the sequence of tricyclic subunits. It follows from this that two isomers that have the same annulation sequence will also have the same NICS-XY-Scan, even if they are geometrically distinct, and this is indeed seen in Figure 2b.

Figure 2. a) Three hexacyclic PBH isomers with their respective notation and annulation sequence and a detailed scheme of the individual tricyclic building blocks contained in them, "reading" left-to-right. b) Plots of the explicitly calculated NICS-XY-scans of the three isomers. **6_13** (pink), and **6_14** (dashed purple) overlap almost exactly, **6_3** (gray) has a different scan curve. Double-bonds are omitted for clarity.

This observation can be seen as a corroboration, or even generalization, of the notion of equiaromaticity coined by Bird and coworkers.[37] According to this notion, polycyclic systems are equiaromatic if the π-currents of their individual rings correspond in a one-to-one manner. Using ring- and bond-currents obtained with a graph-theoretical approach and with Valence Bond calculations, they demonstrated this equiaromaticity between isomers of fibonacenes (in our terminology, these are fully-angularly annulated molecules) and between isomers of heptacyclic lucacenes (in our terminology, these are isomers having an *LAAAA* annulation sequence). As they note in their report, "equiaromaticity arises naturally in the VB picture", however, it is not trivial to assume that it survives the Molecular Orbitals (MO) treatment of electronic structure. The NAdd shows that, not only does the notion exist within the MO treatment, but also that the annulation sequence reveals in a very simple manner which isomers will be equiaromatic.

Methods

Building blocks and test set

The molecules included in the investigation reported herein are depicted in Figure 3. They include PBHs containing from one to six rings, divided into families, where the name of the family is determined by the number of rings in the isomers (e.g., Family 5 contains the pentacyclic isomers considered). The molecules chosen are a selection of the possible isomers in each family (i.e., there are additional isomers we did not calculate), and are considered to be a representative set of each family. Families 1-3 are the building blocks of the additivity schemes and Families 4-6 are the test set for this work.

Figure 3. All molecules investigated in this work, including their respective notation.

Geometries

All geometry calculations were performed using Gaussian 09 Revision D.01.[38] The geometries of all molecules were optimized with the B3LYP[39,40] functional and the 6-311G(d)[41,42] basis set and with the Grimme D3 dispersion correction.[43] Aside from tight optimization thresholds (keyword "opt=tight"), all other parameters were kept in their default settings. Frequencies analysis was performed to ensure true minima on the potential energy surface. Optimization of some of the molecules led to non-planar geometries (these are **5_6**, **6_5**, **6_12**, **6_15**, and **6_16**, which optimize to helical geometries). In such cases, a second optimization was undertaken, in which the starting geometry was made planar. The planarity was then

retained throughout the optimization process. Only planar structures were used in the current work. All optimized geometries are provided in the Supporting Information (SI).

NICS calculations

Explicit NICS-XY-Scan calculations were performed with the Gauge-Including Atomic Orbitals (GIAO)[44,45] method, using the same functional and basis set as the optimizations, to allow for the closest comparison between the NICS values obtained from our implemented procedures. Using the Aroma package,[26,46–48] the NICS(1.7)$_{\pi ZZ}$ metric was calculated with the σ-Only Model.[47] It is important to note that NICS-XY-Scans obtained with Predi-XY (which automates the NICS-XY-Scan additivity scheme) use a library of building blocks for which NICS(1.7)$_{\pi ZZ}$ values were obtained at the B3LYP/6-311+G(d) level of theory, with the Natural Chemical Shielding[49] procedure implemented in NBO 6.0.[50] Based on our experience with these calculations, including several published examples,[26] the difference in values is negligible, allowing for comparison between the different methods. For all molecules in the test set, the NICS-XY-Scans generated with both methods are shown in the SI Section S3.1.

Current densities

The current densities were calculated from the wavefunction (.wfx) file obtained from B3LYP/6-311G(d) calculations with the "output=(wfx,csgt)" keyword, which invoked the Continuous Set of Gauge Transformation (CSGT) method.[51] The π-electron current density data was then calculated from the wavefunction file with the SYSMOIC program.[52] First, the π-orbitals were identified with the MO807xl module, then the JECK module was used to calculate the current density using only the π-orbitals and with a magnetic field perpendicular to the molecular plane (see SI Section S1 for further details).

Bond-current strengths (BCS)

To obtain quantitative and easily interpretable data, we opted to calculate bond-current strengths (alternatively "bond-current susceptibilities") from the current density data, analogously to the procedure employed in the Gauge Including Magnetically Induced Currents (GIMIC) program.[53] Specifically, for each bond, we numerically integrated the current density calculated with JECK on a bond-centered quadrature perpendicular to that bond. We chose a disc quadrature, similarly to the one recently reported in a study by Irons et al.[54] We used the Legendre-Gauss radial quadrature[55] and an evenly spaced angular quadrature with the rectangle rule. Accordingly, the numerical integration was performed according to Equation 1.

$$I_{\mathrm{bond}} \approx R\frac{\theta}{2}\sum_{i}^{n_a}\sum_{j}^{n_r}\omega_j r_j \langle \boldsymbol{j}_{ij}, \hat{\boldsymbol{n}} \rangle \tag{1}$$

where n_a and n_r are the number of angular and radial nodes, respectively; $\theta = 2\pi/n_a$ is the angle between the radial grid lines; *R* is the radius of the disc; ω_j and r_j are the Gauss-Legendre weight and the radial distance for the *j*-th radial point, respectively; $\boldsymbol{j}_{ij}$ is the current vector for the *i*-th angular and *j*-th radial point, and $\hat{\boldsymbol{n}}$ is the normalized normal vector of the disc. We chose the covalent radius of an sp^3 carbon[56] as the disc radius, and placed 10 radial nodes and 20 angular nodes (Figure 4). For reference, our integration gave a BCS value of 5.08 nA T^{-1} for benzene (**1_0**). Expectedly, this is smaller than the BCS value of 11.8 nA T^{-1} calculated with B3LYP and a triple-ζ basis set with GIMIC.[57] As Irons et al reported,[54] BCS values calculated with a disc quadrature are smaller than the respective values calculated with larger integration planes, e.g., the rectangular planes reported in reference [57]. Although the absolute magnitudes are smaller, we expect the relative magnitudes to be reliable. In our data, the ratio between the circumference current strength in **2_0** and **1_0** is 1.09, similar to the ratio reported by Irons et al (1.10-1.13, depending on the method)[54] and McWeeny (1.09).[20]

Figure 4. Example of the disc quadrature on a bond in benzene (**1_0**), shown in top view (left) and tilted view (right). The points at which the current was calculated are shown in pink.

NICS from the Biot-Savart equation

$NICS_{ZZ}$ (the variant of NICS that we use in this work) at a point $\boldsymbol{r}$ is defined as the negative of the *ZZ* component of the chemical shielding tensor at that point.

$$\boldsymbol{\sigma}(\boldsymbol{r}) = \begin{pmatrix} \sigma_{XX}(\boldsymbol{r}) & \sigma_{XY}(\boldsymbol{r}) & \sigma_{XZ}(\boldsymbol{r}) \\ \sigma_{YX}(\boldsymbol{r}) & \sigma_{YY}(\boldsymbol{r}) & \sigma_{YZ}(\boldsymbol{r}) \\ \sigma_{ZX}(\boldsymbol{r}) & \sigma_{ZY}(\boldsymbol{r}) & \sigma_{ZZ}(\boldsymbol{r}) \end{pmatrix} \tag{2}$$

The chemical shielding tensor relates to the induced magnetic field $\boldsymbol{B}^{\text{ind}}(\boldsymbol{r})$, which arises from the current density induced by an external magnetic field $\boldsymbol{B}^{\text{ext}}$. For a uniform external magnetic field, the relationship is:[35]

$$\boldsymbol{B}^{\text{ind}}(\boldsymbol{r}) = -\boldsymbol{\sigma}(\boldsymbol{r})\boldsymbol{B}^{\text{ext}} \tag{3}$$

$\boldsymbol{B}^{\text{ind}}(\boldsymbol{r})$ can be calculated by integrating the differential Biot-Savart equation.[58] In case the current is defined on a line, as is the case with bond-currents, the integral is a line integral:

$$\boldsymbol{B}^{\text{ind}}(\boldsymbol{r}) = \frac{\mu_0}{4\pi}\int_C I(\boldsymbol{r}')\frac{d\boldsymbol{l}\times(\boldsymbol{r}-\boldsymbol{r}')}{|\boldsymbol{r}-\boldsymbol{r}'|^3} \tag{4}$$

where $I(\boldsymbol{r}')$ the current strength at $\boldsymbol{r}'$, $d\boldsymbol{l}$ is a differential vector along the current path *C*, and μ_0 is vacuum permeability. There are several examples of using bond-currents instead of the full current density to calculate the induced magnetic field by the Biot-Savart equation, dating back to the late 1950s.[20,59,60] We

used a similar approach, in which we approximated the integral by calculating the contribution from all of the N bond-currents, each of which we discretized into M evenly spaced grid points (intervals of $\Delta \boldsymbol{l}$) with the same current value I_{bond}.

$$\boldsymbol{B}_{\mathrm{ind}}(\mathbf{r}) \approx \frac{\mu_0}{4\pi} \sum_{i}^{N} I_{\mathrm{bond_i}} \sum_{j}^{M} \frac{\Delta \boldsymbol{l} \times \left(\boldsymbol{r} - \boldsymbol{r}_j'\right)}{\left|\boldsymbol{r} - \boldsymbol{r}_j'\right|^3} \tag{5}$$

As our absolute magnitudes of BCSs (and thereby I_{bond}) are smaller than the "true" ones, but the ratios between different BCSs are expected to be correct, we decided to scale the BCS values to more realistic magnitudes prior to the $\boldsymbol{B}^{\mathrm{ind}}(\boldsymbol{r})$ calculation. We applied a constant scaling factor such that the BCS value for benzene (**1_0**) would be 11.7 nA T^{-1}, as calculated for the π-electron current by Monaco et al.[61] Although the computational method used for our current density field calculations differs from that of Monaco et al, we expect the influence of the method to be less significant than that of the size of the integration grid, based on the data by Irons et al.[54]

To obtain the NICS-XY-Scans, we followed the conventional NICS-XY-Scan protocol by placing NICS probes along a pathway connecting the centers of the rings and the centers of the fused bonds, with 0.1 Å intervals, at a constant height above the molecular plane. For each probe, we calculated the induced magnetic field based on our numerical approximation of Biot-Savart's law (Equation 5, with M = 100) and calculated $\mathrm{NICS}_{\mathrm{ZZ}}$ as:

$$\mathrm{NICS}_{\mathrm{ZZ}}(\boldsymbol{r}) = -\sigma_{ZZ}(\boldsymbol{r}) = \frac{B_{\mathrm{ind,Z}}(\boldsymbol{r})}{B_{\mathrm{ext,Z}}} \tag{6}$$

We found the optimal scan height of 1.15 Å by minimizing the root-mean-square deviation (RMSD) between the NICS-XY-Scans calculated for the whole test set by Equation 6 and the respective explicit NICS-XY-Scans as described in "NICS calculations", using the Brent method.[62] Note that, because only the π-orbitals were used to obtain the current density data, these are $\mathrm{NICS(r)}_{\pi ZZ}$ values. Thus they can be compared to the $\mathrm{NICS(1.7)}_{\pi ZZ}$ values obtained with the explicit calculation.

We used an in-house Python code to perform the current density integration and the Biot-Savart calculation; the numerical operations were performed with standard NumPy[63] and SciPy[64] tools.

The Bond-Current Strengths Additivity Scheme (BAdd)

We define the BAdd scheme analogously to the NAdd scheme (see The NICS-XY-Scan Additivity Scheme (NAdd) section), i.e., we identify monocylic, bicyclic, and tricyclic subunits in a PBH, and combine their superimposed contributions based on the sequence in which they appear in the molecule. The main technical difference between the two schemes is that, whereas in the NAdd we can simply sum up the superimposed

arrays of the individual contributions, for the BAdd every bond in the subunit must be mapped to the respective bond in the larger molecule. To handle this procedure in an automated manner, we wrote an in-house Python code using the NetworkX package.[65] In short, the code generates a graph for the molecule of interest, using the list of atoms to define the nodes, and the respective Cartesian coordinates and the covalent radii to identify the connectivity and thereby define the edges (bonds). The monocyclic, bicyclic, and tricyclic subunits are then identified within the molecule and set as subgraphs of the molecular graph. For each subgraph, the respective building block is selected by testing for isomorphism, and the respective pre-calculated BCS values are mapped to a directed graph of that subunit. From those directed graphs, the bicyclic and tricyclic corrections are calculated on-the-fly using the same definition as in the NAdd. In the last step, a directed graph of the molecule of interest is generated where the weight (BCS) for each edge (bond) is calculated by adding together the respective values of the subgraphs, i.e., the monocyclic contributions, the bicyclic corrections, and the tricyclic corrections.

Visualization

The 3D molecular representations were visualized with Pymol (version 1.7.4).[66] The BCS plots and NICS-XY-Scan plots were generated with Matplotlib.[67] The direction of the current in the BCS plots is defined as the positive current, with the external magnetic field perpendicular to the plane of the molecule and pointing into the plane. The NICS-XY-Scans are plotted as lines for clarity, although the data consist of discrete data points, spaced by approximately 0.1 Å on the abscissa.

Results

Throughout this text we compare results obtained with different methods of calculation. For clarity, we list here the terminology we used in the text:

- BC^{ref} – Bond-current strengths obtained by integration of DFT-calculated current density.
- BC^{BAdd} – Bond-current strengths obtained with the bond-current additivity scheme (BAdd).
- $NICS^{ref}$ – NICS values calculated explicitly with DFT.
- $NICS^{NAdd}$ – NICS value calculated with the NICS-XY-Scan additivity scheme (NAdd).
- $NICS^{BC}$ – NICS values calculated with the Biot-Savart law on the basis of BC^{ref} values.
- $NICS^{BAdd}$ – NICS value calculated with the Biot-Savart law on the basis of BC^{BAdd} values.

In addition, we note that, for conciseness, we do not present here the results for all of the compounds in the test set. Rather, we have selected six representative compounds—**6_0**, **6_2**, **6_6**, **6_7**, **6_9**, and **6_10**—which contain all of the structural motifs relevant for the analysis of the results. The data for all of the molecules are provided in the SI and are consistent with the conclusions described in this text.

The Bond-Current Strengths Additivity Scheme (BAdd)

The BCSs were calculated by integration of the current densities (see Methods section for further details). Using the calculated BCSs, we constructed the Bond-Current Strengths Additivity Scheme (hence, the BAdd) analogously to the NAdd. In Figure 5a we display the building block library of the BAdd method. The values of benzene (**1_0**) are used as-is, as they form the basis of the predicted value for the larger PASs. As described above, the bi- and tricyclic components are considered via correction terms, which are calculated as the difference (BC^{ref} –BC^{BAdd}). We show in Figure 5b the results of these two metrics and the resulting correction, depicted as arrows placed on the respective bonds, where the size of the arrow represents the magnitude of the BCS (the arrows of the correction terms are scaled by a factor of 5 to make them clearly visible). For the correction terms, the color of the arrow represents the direction of the current, where the direction of the BC^{ref} for each bond is considered to be the positive direction. Accordingly, green arrows are a result of positive errors ($BC^{ref} – BC^{BAdd} > 0$) and purple arrows indicate negative errors ($BC^{ref} – BC^{BAdd} < 0$).

Figure 5. a) The building block library of the BAdd: benzene (**1_0**), naphthalene (**2_0**), anthracene (**3_0**), and phenanthrene (**3_1**). b) BC^{ref} (dark blue) and BC^{BAdd} (light blue) for the bi- and tricyclic building blocks, and the respective correction terms (calculated as $BC^{ref} – BC^{BAdd}$). Green arrows show positive corrections; purple arrows show negative corrections. The corrections are scaled by a factor of 5 and double-bonds are omitted in all figures for clarity.

Using these building blocks and the combination rules we previously described for the NAdd, we constructed the predicted BCSs of the larger molecules (containing from four to six rings). In Figure 6 we compare BC^{ref} and BC^{BAdd} values for the six representative molecules, and also display the difference between the two.

Figure 6. Comparison of the BCS values obtained with BC^{ref} (dark blue) and BC^{BAdd} (light blue). The difference between the two (third column from the left, arrows scaled by a factor of 5) is shown to demonstrate the closeness of the two methods. Green arrows show positive errors; purple arrows show negative errors.

NICS-XY-Scans obtained with BAdd-generated bond-currents ($NICS^{BAdd}$)

We then used the Biot-Savart law to obtain NICS values from the BCSs (see Methods section for further details). Figure 7 displays the results of several calculations for the six representative molecules (for data for all molecules in the test set, see SI Section S2.1). Each plot describes the results for one particular molecule, divided into two sets: BAdd (blue) and NAdd (black/gray). The blue set includes $NICS^{BC}$, $NICS^{BAdd}$, and the difference between these two scans. The black/gray set includes $NICS^{ref}$, $NICS^{NAdd}$, and the difference between these two scans (for the definitions of each acronym, see the beginning of the Results

section). The two solid curves are the respective reference values for each set, and the difference curves are the respective error values, by which we can evaluate the performance of the BAdd and NAdd.

Figure 7. Comparison between the NICS-XY-Scans generated with the constructed additivity methods and their respective reference scans.

Based on visual inspection of the results of BC^{BAdd} and $NICS^{BAdd}$, we divided the molecules into five sets: 1) fully angularly-annulated molecules; 2) molecules containing linear annulation stretches no longer than three rings; 3) molecules containing linear annulation stretches of four rings or longer; 4) fully linearly-annulated molecules; 5) molecules containing the *LAL* annulation sequence. Table 1 details the molecules contained within each set. For each set, we report the mean unsigned error (MUE) calculated for all molecules in that set, as well as the single maximal error observed among the set (for MUEs of the individual molecules, see Table S3 in the SI). All of the values are reported as a ratio relative to the reference value of benzene. Compound **6_1** was placed in Sets 3 and 5, as it fits the structural criteria for both.

Table 1. Relative errors in the BAdd method for each of the sets of molecules. Expressed as a ratio to the value calculated by the same method for benzene.

Set	**Relative BC^{BAdd} error**[a]		**Relative $NICS^{BAdd}$ error**[b]		**Molecules in Set**
	MUE[c]	Max. Error[d]	MUE[e]	Max. Error[f]	
1	0.05	0.16	0.05	0.13	**4_2**, **5_4**, **6_10**, **6_12**, **6_15**
2	0.05	0.21	0.04	0.14	**4_1**, **5_1**, **5_3**, **5_6**, **6_9**, **6_11**, **6_13**, **6_14**, **6_16**
3	0.09	0.36	0.07	0.31	**5_5**, **6_1**, **6_2**, **6_3**, **6_5**, **6_6**, **6_8**
4	0.13	0.32	0.11	0.31	**4_0**, **5_0**, **6_0**
5	0.10	0.36	0.09	0.31	**5_2**, **6_1**, **6_4**, **6_7**

[a] values reported as a ratio w.r.t to the reference value for benzene (5.1 nA T^{-1})
[b] values reported as a ratio w.r.t to the reference value for benzene (–16.6 ppm, in the middle of the ring)
[c] MUE of BC^{BAdd} w.r.t. BC^{ref}
[d] maximal BC^{BAdd} error in set
[e] MUE of $NICS^{BAdd}$ w.r.t. $NICS^{BC}$
[f] maximal $NICS^{BAdd}$ error in set

Discussion

Before we turn to discussing the results presented in this report, we wish to put this investigation into the appropriate context. The field of research dealing with ring-currents in aromatic systems is wide and varied, including multiple methods for computation of current densities and multiple suggestions for how to understand aromaticity based on these currents. A complete survey of these works is not in the scope of the current paper, however, we do wish to point out previous reports that specifically focused on two issues: a)

the notion of additivity with currents and b) the use of BCSs in PASs, because these are highly relevant to this text.

Firstly, we address the issue of additivity. Though our NAdd method was the first demonstration of additivity with NICS, the idea of additivity within PASs is not new. In the 1970s, Randić introduced the "conjugated circuits model" (CCM),[68–70] whereby one identifies all possible circuits made of alternating single and double bonds in conjugated hydrocarbons. According to the CCM, systems containing only (4n + 2) circuits are aromatic, those containing only (4n) circuits are antiaromatic, and those containing both types are intermediate (partially aromatic). A few years after the method was introduced, Gomes[71] demonstrated that the conjugated circuits behave in an additive manner, which he termed a "non-empirical system of increments". Moreover, he showed that the conjugated circuits could be used to obtain properties such as resonance energies and ring-currents. More recent work has used the framework of the CCM in combination with a wavefunction ansatz to determine London susceptibilities and ring-current intensities with high accuracy.[72] For many years, the Aihara group has been developing a graph theory of aromaticity and diatropicity, leading to the introduction of metrics such as TRE[73] and CRE[74] (topological- and circuit-resonance energy, respectively). As with the Randić model, Aihara's approach does not break the molecules into structural components, but rather, identifies possible circuits within the total structure. These are seminal contributions that put forth the notion that identifying parts within a polycyclic system could aid in characterizing the system, as a whole. For further reading, one may refer to the recent study by Hamzah et al, which uses a test set of benzenoids containing 1-7 rings to compare two CCM versions with the graph-theoretical Hückel-London model.[75] Bultinck and coworkers also made use of the subcircuit notion, but focused on specific types, e.g., six-, ten-, or fourteen-center circuits to find correlation between ring-currents and multi-center bond indices.[76] A special case of additivity is known as the "annulene within an annulene" model, in which a single PAS sustains separate rotational fields on two or more subunits within the structure (i.e., the π-current is separable into contributions that are largely localized on some subunits). In such cases, the circuits do not affect one another and therefore the total current density of the larger PAS can be described as the sum of the individual components, i.e., as additive.[77] Candidates for such behavior are the *altan*-molecules,[78] which are characterized by an inner annulene ring connected to an outer annulene ring via spokes (e.g., corannulene, coronene). Several recent publications have investigated the topological ring currents in *altan* systems.[79–81] The current flows along each of the annulenes, but not on the spoke bonds, thus many of the molecules in this family exhibit additivity of current density[82] and of ring- and bond-currents.[83] To the best of our knowledge, the additivity of *altans* has not been demonstrated quantitatively. Rather, it is more a conceptual pursuit, dedicated to identifying structures that display this behavior and finding characteristics of the additive behavior (e.g., a saddle point in the current density). Moreover, the individual components are unique to each molecule, so the model is not universally

applicable. Thus, the BAdd method is unique in several aspects: a) it deconstructs the molecule into smaller structural components, b) it uses a small, fixed-size library for all compounds, c) it affords a quantitative prediction of the property of the studied compound.

Secondly, we address the issue of BCSs. To construct an additivity scheme for the induced current density, we first needed to determine how to represent it. As described very aptly by Jusélius and Sundholm, "though the current density is a proper quantum mechanical observable… current density plots do not provide any quantifiable measures of the current strengths nor are they suitable for comparing current strengths in different molecular systems".[53] In addition, we required a method that could be mapped easily to the structure of the PBH (specific bonds), to allow for easier mathematical treatment, i.e., addition and subtraction of effects. Therefore, we chose to use bond-current strengths (BCSs) as a model for the induced current density. Early examples of using of bond-currents (in place of the current density) for calculating the induced magnetic field with Biot-Savart's law were reported approximately 70 years ago by McWeeny[20] and Longuet-Higgins.[59] Ring-currents, which are an alternative method of describing currents in PASs, are also commonly used. Lazzeretti and coworkers reported on a ring-current model, in which they described the flow of electrons in a conjugated system by modeling it as an infinitely thin and perfectly circular conducting loop, and then used Biot-Savart's law to integrate the current and obtain NICS values.[84] In a separate paper, they describe construction of ring-currents from homotropic local vortices.[85] Mallion and coworkers have used both ring- and bond-currents extensively,[60,86,87] and specifically emphasize the value of considering bond-currents when investigating π-electron magnetic properties in PASs.[83] Thus, the use of BCSs is well-established in the literature and brings with it several advantages that make it suitable for our goals.

In this section, we interpret and discuss the Results presented above, focusing on the accuracy of the implemented procedures, the quality of the BAdd method, the agreement between the NAdd and BAdd methods, and the possible causes for error in the BAdd method.

Accuracy of the implemented procedures

The first step of our analysis was to verify that our constructed procedure (integration of current density to give BCSs, followed by application of Biot-Savart's law) is capable of correctly reproducing the magnetic response of the PBHs. To ensure an accurate comparison, we addressed three issues: a) which orbitals are considered, b) which components of the chemical shift tensors are considered and c) where the NICS probes are located relative to the current. For calculating $NICS^{ref}$, we used the $NICS(1.7)_{\pi ZZ}$ metric obtained with the σ-Only Model.[47] This means that the probes were placed 1.7 Å above the molecular plane, only the ZZ component of the chemical shielding tensor was considered and, to a good approximation, only the contributions of the π-electrons were considered. Therefore, to ensure similarity, in our procedure we used

only the current density resulting from the π-orbitals and then used only the ZZ component of the resulting chemical shielding tensor obtained with the Biot-Savart equation (Equation 5). Thus, the only issue remaining was the location of the probes. The explicit calculation for $NICS^{ref}$ placed the probes at the conventional height of 1.7 Å above the molecular plane. Because the BCS model reduces the 3-dimensional current density to a 2-dimensional representation, the optimal location (height) of the probes is expected to change. To find the best height, we performed an optimization of the RMSD between $NICS^{ref}$ and $NICS^{BC}$ and found the optimal height to be 1.15 Å. Though this is just a fit parameter in our procedure, it does comport with our expectation that the probes should be closer to the molecular plane, where the BCSs are located. We emphasize that once the optimal value was determined, all $NICS^{BC}$ and $NICS^{BAdd}$ values were calculated at the same height.

The success of the implemented procedure is demonstrated in Figure 7 with the comparison between $NICS^{ref}$ (solid black) and $NICS^{BC}$ (solid blue). As seen in the plots, in all examples, these lines show a remarkable agreement. From this we can conclude that the procedure we constructed can safely be used to model the actual induced currents in PBHs, and that the NICS-XY-Scans generated by our code faithfully reflect the BCSs sustained in the systems. The ability of the model to reproduce NICS values as accurately as it does is even more remarkable, given the simplifications introduced.

Quality of the BAdd

The BAdd can be assessed on two levels: a) its ability to reproduce the BCSs obtained based on DFT calculations (BC^{ref}) and b) its ability to reproduce the explicitly calculated NICS-XY-Scans ($NICS^{ref}$).

We first address the ability of the BAdd to reproduce accurate BCSs. We show in Figure 6 the agreement between the BC^{ref} and BC^{BAdd} by representing the current with arrows, wherein the size of the arrow correlates to the magnitude of the BCS on that bond. Visual inspection of the six representative molecules shows that the BC^{BAdd} arrows (light blue) look very similar to the BC^{ref} arrows (dark blue), but there are subtle differences in arrow size. To visualize the agreement more easily, we display the difference between the two calculation methods in the right-hand column, which can be considered as the error of the BAdd (the arrows in this column are enlarged by a factor of 5 to make the effects more clearly visible). In our color coding scheme, green arrows indicate BCSs for which $BC^{ref} > BC^{BAdd}$ and purple arrows indicate BCSs for which $BC^{ref} < BC^{BAdd}$. Because all of the molecules studied here are aromatic and are characterized by diatropic currents, green (purple) error arrows indicate that the BAdd method underestimated (overestimated) the diatropic current in that location. The BC^{ref}, BC^{BAdd}, and error data for all molecules is presented in the SI Section S2.2.

In general, visual comparison between BC^{BAdd} to BC^{ref} plots shows that the BAdd method reproduces the BCSs well. This is corroborated by the fact the BC^{BAdd} values for all 27 molecules consisting of four to six benzene rings have a MUE = 0.07 (expressed as a ratio w.r.t. to the reference value of benzene). As described above, visual inspection of the resulting plots revealed that certain structural motifs tend to have larger errors than others, leading us to divide the data into five sets. We detail the observations leading to this decision here: For **4_0**, **5_0**, and **6_0**, the errors consistently appear as green arrows in the middle part of the molecule (i.e., the BAdd underestimates the strength of the diatropic current flowing around these rings; see Figure 6 and SI Section S2.1). Due to symmetry, in **4_0** and **6_0**, the error encompasses the middle two rings; for **5_0** the error is largest in the middle ring. This is repeated in the molecules that are not fully linearly annulated, as well (e.g., **6_1**). When longer linear substructures (i.e., four or more rings) are adjacent to an angular substructure, similar trends are seen in the linear stretches—the BCSs of the middle rings are noticeably underestimated—and in addition the diatropic current in the middle ring the angular (i.e., phenanthrenic) subunit is overestimated by the BAdd, as denoted by purple arrows. For the *LAL* motif, seen in **5_2**, **6_1**, **6_4**, and **6_7**, the diatropic currents are overestimated in the phenanthrene subunit (purple error arrows) (see Figure 6 and SI Section S2.1). These repetitive patterns indicate that the BAdd does not capture some of the subtler nuances of specific PBH structural motifs, and that the accuracy is linked to particular structural motifs.

To probe this further, we divided the molecules into sets and analyzed the accuracy of the method w.r.t. these sets. Table 1 details the errors for the different sets (for MUEs of the individual molecules, see SI Table S3). The MUEs of the different sets follow the trends observed from the visual inspection. The molecules in Set 1 and Set 2 show the smallest average error, MUE = 0.05 for both sets, as well as the smallest maximal error, max error = 0.15 and 0.21, observed for **6_12** and **6_16**, respectively. The error increases when the length of the linear stretch in the molecule elongates, as seen for Set 3 (MUE = 0.09). This trend continues, culminating in the largest errors being observed for the compounds in Set 4 (MUE = 0.13). There is also a specific annulation sequence, *LAL*, which appears to challenge the model, which is seen in the results for Set 3 (MUE = 0.10). The molecule with the highest maximal error is **6_1** (max error = 0.36), which contains not only a tetracyclic linear stretch but also an *LAL* sequence. These quantitative error data support our previous conclusion, which was based on visual inspection, that there is a relationship between structural features and the performance of the method.

To evaluate the performance of the BAdd with respect to reproducing NICS-XY-Scans, we compare the $NICS^{BAdd}$ (dashed blue) to $NICS^{BC}$ (solid blue), seen in Figure 7. Visual inspection of the plots suggests that the BAdd provides the basis for satisfactory NICS-XY-Scans. The $NICS^{BAdd}$ scans generally follow the reference curves of $NICS^{BC}$ well, matching the trends and local minima/maxima. The curves of the

difference between these two methods (dashed-dotted light blue), which serve as a quantitative indication of the agreement, lie for the most part in the range ±2 ppm, with maximal errors reaching approximately ±5 ppm (0.13 and 0.31, respectively, when expressed as a ratio w.r.t. to the value calculated for benzene with the same method). Not surprisingly, the MUEs for $NICS^{BAdd}$ are close in range to those for BC^{BAdd} (between 0.05 – 0.13), and they follow the same trends observed before, in terms of the structural motifs and division into sets. Sets 1 and 2 have the lowest errors (MUE = 0.05 and 0.04, respectively); the error for Set 3 is higher (MUE = 0.07), continuing to even larger errors in Set 4 (MUE = 0.11); and the error for Set 5, the molecules containing the *LAL* motif, is somewhere between Sets 3 and 4 (MUE = 0.09). **6_1** is again the molecule with the highest individual error, max error = 0.31.

The division into sets of molecules allows us to identify certain relationships between structural motifs and the accuracy of the method, which we summarize here. Firstly, it appears that Sets 1 and 2 are described with comparable accuracy, i.e., though there are structural distinctions between them, these do not appear to change the way they are treated by the BAdd method. Accordingly, the method achieves its maximum accuracy in treating molecules having no linear stretches at all and those having a tricyclic linear stretch. We note also that having two separate tricyclic linear subunits does not seem to increase the error, e.g., for **6_9**, MUE = 0.04 and 0.03, for BC^{BAdd} and $NICS^{BAdd}$, respectively. Secondly, more noticeable deviations appear when there are linear stretches longer than four rings, and these deviations increase as the linear stretch increases in length. Thirdly, the *LAL* sequence is a specific substructure that stands out as being poorly described with the BAdd method.

Agreement between the NAdd and the BAdd

In the previous subsection we assessed the performance of the BAdd in reproducing the BC^{ref} and $NICS^{BC}$ of the systems in our test set (we note that, due to the close matching of $NICS^{BC}$ and $NICS^{ref}$, this indicates that $NICS^{BAdd}$ also reproduces $NICS^{ref}$ well). The final comparison we want to explore is that between the NICS-XY-Scans generated by the two additivity schemes. i.e., $NICS^{NAdd}$ and $NICS^{BAdd}$. As mentioned in the introduction, the initial motivation behind this study was to corroborate the NAdd results with the underlying property, i.e., the current density. If indeed the additive behavior implied by the NAdd is linked to an underlying additivity of current density (modeled here with BCSs), then the results of the two schemes should agree. In Figure 7 the NICS-XY-Scans of the six representative molecules, obtained with the two methods, are shown ($NICS^{BAdd}$ in dashed blue, $NICS^{NAdd}$ in dashed gray) and can be seen that the agreement between the two is excellent (data for all molecules in the test set is provided in Section S3.1 of the SI). Additional proof that the NAdd is closely linked to the underlying BAdd is that their errors coincide. This is seen by the difference curves (light blue and light gray, respectively), which show the errors of each

scheme relative to its respective reference. These error curves show that the two schemes agree very well, both in the areas that they model well and in those that they struggle to describe accurately.

To further strengthen our observation of correspondence between the NAdd and BAdd, we compare the results of $NICS^{NAdd}$ with BC^{BAdd}. For each ring in each molecule, we calculated the average of BC^{BAdd} errors (i.e., the average of the individual errors for each of the BC^{BAdd} values in a given ring expressed as a ratio w.r.t. to benzene) and plotted these values as bars, where the color of each bar matches the sign of the error (green when $BC^{ref} > BC^{BAdd}$, purple when $BC^{ref} < BC^{BAdd}$) and the position of the bar corresponds to the location of the ring along the distance axis in Å. Against these bars, we plotted the $NICS^{BAdd}$ and $NICS^{NAdd}$ errors (i.e., the light blue and light gray curves from Figure 7), expressed as a ratio w.r.t. to the reference value of benzene. In Figure 8 we display two cases, **6_2** and **6_9**, which represent cases of less and more accurate prediction by the models, respectively (the same plots for all of the molecules are provided in Section S4.1 of the SI). We observe that the errors in the NAdd correspond very closely to those in the BAdd, both in magnitude and in the direction of the error (over- or underestimation). Note that the BC^{BAdd} errors are reported in the opposite sign. The reason is that the two metrics are reported with opposite mathematical signs: a stronger induced ring-current will give a more positive BC^{BAdd} and a more negative $NICS^{BAdd}$. As a result, for an overestimated (underestimated) ring-current, the BC^{BAdd} errors will be negative (positive) and the $NICS^{BAdd}$ errors will be positive (negative). To more clearly compare the two, one of the metrics must be "flipped" and we arbitrarily chose the BC metric.

Figure 8. Comparison of errors in the BC^{BAdd}, $NICS^{BAdd}$, and $NICS^{NAdd}$ metrics. All errors expressed as a ratio w.r.t. to the respective reference value for benzene. BC^{BAdd} errors are reported with the opposite sign.

From Figure 7 we make the additional observation that the two schemes differ in the fine features of the scans. The $NICS^{NAdd}$ scans appear smoother than the $NICS^{BAdd}$ scans, which often have small fluctuations, or "waves" (e.g., in **6_10**, Figure 7). These waves appear also in the reference scans, but $NICS^{NAdd}$ scans fail to reproduce these fine details, while the $NICS^{BAdd}$ scans do. As a result, the error curve for the NAdd appears bumpy and the BAdd error curve is smoother (seen in Figure 8). The locations of the waves generally coincide with the location of the fused bonds (this can be understood from Figure 8, where the two metrics agree at the centers of the ring, but the $NICS^{NAdd}$ has spurious extrema between ring centers).

Causes of error and limitations of the schemes

The results discussed in the previous subsections demonstrate that the additivity we previously observed with NICS-XY-Scans is indeed echoed in the underlying behavior of currents, and both schemes, NAdd and BAdd, reproduce the explicitly calculated results remarkably well. Though we were gratified to see the

overall performance of the schemes, our attention was drawn to the more challenging cases, where both schemes struggle. While predictive models can be useful, they can only be employed safely when one is aware of the limitations of the model. Moreover, as the errors in these cases seemed to be tied to specific structural motifs, we were intrigued to understand their origin better.

Our approach to doing so was to remove the bi- and tricyclic building blocks from the additivity scheme. In other words, to use only monocyclic subunits (i.e., benzene) in the construction of the larger PBHs. This was prompted by two observations: a) Figure 5a shows that the bi- and tricylic corrections are barely noticeable, compared to the monocyclic BCS, giving the impression that these larger building blocks may be unnecessary and b) the additivity schemes appear to perform better with all-angular sequences, suggesting that there might be a problem with the description of the linear subunits.

If only monocyclic building blocks are used, then, by definition, all PBH isomers will have the same BCSs. Furthermore, there will be bond-currents only on the circumference bonds, because, by symmetry, all currents on the fused bonds will be cancelled out. We refer to this as the "uniform-current" model, and the NICS-XY-Scans resulting from its application to the representative molecules are presented in Figure 9 (results for all molecules in the test set are provided in Section S3.2 of the SI).

Figure 9. Comparison of the NICS-XY-Scan obtained from the uniform-current model (yellow) to the $NICS^{BC}$ scans (blue) for the six representative compounds.

Several observations can be made on the basis of Figure 9. First and foremost, we can conclude that this model does not reproduce the $NICS^{ref}$ values well, i.e., using only monocyclic building blocks is not sufficient for constructing an additivity scheme and the additional bicyclic and tricyclic corrections are necessary. Thus, the results of the uniform-current model clearly show that, though these corrections are substantially smaller than the base value (as seen in Figure 5a), they determine the features of the BCSs and NICS in the molecule. Moreover, they play a critical role in differentiating between isomers.

Secondly, we note that the molecules of Set 1 (fully angularly-annulated molecules, namely, **4_2**, **5_4**, **6_10**, **6_12**, **6_16**; the data for **6_10** is shown in Figure 9, and for the rest of the set in Section S3.2 of the SI) are the only ones that show an acceptable agreement between $NICS^{ref}$ and the NICS-XY-Scan from the uniform-current model. What sets these molecules apart from the other sets is that they all have very small currents on the fused bonds (see Figure 6) and, according to the continuity equation (or, in analogy to electrical circuits, Kirchhoff's First Law),[58] therefore also have a rather consistent current strength at the circumference. This kind of behavior is extremely similar to the uniform-current model, which explains why this model reproduces the $NICS^{ref}$ scans remarkably well for these systems.

Thirdly, we observe that the uniform-current model generates essentially identical NICS-XY-Scans for all isomers, regardless of their structure. Simplistically, we can think of the different isomers as wire loops, sustaining identical currents, which have been bent into different shapes. The fact that they all afford effectively indistinguishable plots therefore implies that it is not the geometrical shape of the current that determines the features of the scan.

Put simply, we consider the largest contribution of this model to be its clear demonstration of the necessity of the larger building blocks, which is a corroboration of our choice of building blocks in the additivity methods. Furthermore, it does clarify the importance of the currents on the fused bonds and of the fluctuations in strength of the circumference current in determining the magnetic features of the molecules. Aside from this, this model mostly reiterates previous conclusions—the additivity schemes work better for the all-angular molecules and the deviations are linked to the linear stretches—and does not provide additional clarity into why this is so.

A possible explanation for the difficulty in describing linear stretches with additivity can be found in the work of Szczepanik and coworkers.[88] Similarly to us, they observed (with various aromaticity indices) that the difference between side and middle rings increases as the length of the linear polyacene increases. They concluded that, for linear polyacenes, inter-ring resonance effects play a key role in determining the distribution of current density and these effects could be modeled accurately by solving a system of simple linear equations. Another way to frame this, in the context of our own results, would be to say that angular subunits retain their characteristic behavior regardless of the larger structure in which they appear, while linear subunits are impacted by their environment. This is echoed in other electronic properties, as well. As reported widely in the literature, for polyacene molecules (fully linearly annulated PBHs) the HOMO-LUMO gap decreases with the increase in number of rings,[89] which is similar to the relationship seen in polyenes, and suggests that there is extended conjugation. In contrast, the polyphenacenes ("zig-zag" isomers of PBHs) have a relatively consistent HOMO-LUMO gap, even when the chain is extended substantially.[90]

To summarize these observations in terms of the additivity schemes we have constructed, we conclude that the fully-angular systems and the systems containing linear stretches no longer than three rings are the most accurately predicted, and that an increase in the length of linear stretches (four rings and longer) leads to poorer accuracy. Specifically, for molecules including such substructures, while the trends will most likely be correctly found (local minima and maxima), the exact BC^{BAdd}, $NICS^{BAdd}$, and $NICS^{NAdd}$ values will not match the reference values. These conclusions raise two additional questions: a) how do the errors scale with the size of the molecule, and b) does the inaccuracy arising from a linear stretch mean that the entire molecule is not modeled accurately.

To answer these questions, we considered some larger systems. In Figure 10 we reproduce results from our recent report, which demonstrated the use of the automated code Predi-XY to predict NICS-XY-Scans based on the NAdd.[34] We chose three PBHs, containing seven to ten rings, denoted **8**-**10.** The $NICS^{NAdd}$ for these systems results can now be viewed in light of the conclusions outlined above, and we observe that they remain valid for larger systems as well. Compound **9**, which is fully angularly-annulated, and compound **10**, which contains both linear and angular subunits, both show good agreement between the $NICS^{ref}$ and $NICS^{NAdd}$ scans. This corroborates our previous conclusions that the method deals well with angular annulations and with linear stretches of three rings. However, if two linear tricyclic subunits happen to be part of an *LAL* sequence, as in **8**, this does indeed lead to larger error, as we outlined above. Moreover, we observe that these errors are localized, i.e., the other areas of these molecules (e.g., the rings outside the *LAL* sequence in **8**) are modeled well. Therefore, to answer the two questions posed above: a) the error margins we described above (average error ~2 ppm, maximal error ~5 ppm) hold true for the larger systems and do not increase with the size of the system; b) no, inaccuracies arising from poorly-modeled areas do not lead to the entire scan being wrong.

The answer to question (b) warrants further discussion. The NAdd, by definition, precludes any effect farther than two rings away from a given ring, because it only uses components up to tricyclic subunits. However, the actual behavior of the system may, in principle, have long-range effects. The fact that we observe lack of dependency between the "problematic" and "well-modeled" areas strengthens our hypothesis that the main characteristics of PBHs—location of local extrema and magnitude of the NICS metric—are governed by short-range effects, and that they behave additively. It also serves to highlight that, although the predictions made by the schemes are quite satisfactory, further improvement could be achieved by describing the linear subunit better, perhaps through weighting the values in a linear stretch when the stretch exceeds three rings or by incorporating the inter-ring effects, as suggested in reference [88]. These are avenues that we are continuing to explore.

Figure 10. Comparison of $NICS^{ref}$ and $NICS^{NAdd}$ for three larger PASs test compounds: **8**, **9**, and **10**.

Conclusions

The present study was motivated by a desire to understand the origin of the additive nature of NICS-XY-Scans and to provide a sounder physical basis for these observations. To investigate this, we constructed a BCS model of the current density and implemented a BCS additivity scheme (BAdd), analogous to the original NAdd. We tested the BAdd method's behavior as an additivity scheme in its own right and showed that the BAdd is capable of reproducing the explicitly calculated BCSs (BC^{ref}) well. In addition, $NICS^{BAdd}$

scans generated on the basis of BC^{BAdd} values match both the NICS-XY-Scans generated from BC^{ref} and those calculated explicitly ($NICS^{ref}$). Finally, we demonstrated that the $NICS^{BAdd}$ scans agree very closely with the $NICS^{NAdd}$ scans. The entirety of our results overwhelmingly support the conclusion that the NAdd does stem from an underlying additivity, which occurs on the level of the induced current density.

We probed the accuracy of the methods on our test set, finding MUE = 0.07 for BC^{BAdd} and MUE = 0.06 for $NICS^{BAdd}$ (expressed as a ratio w.r.t. to benzene), and reporting also the maximal error found in our test set, 0.36 and 0.31, respectively. We identified the specific structural motifs that prove most challenging for the models and for which the error reaches these maximal values—the *LAL* sequence and linear stretches longer than three rings. We showed that these upper boundaries for error are stable even when the systems are further extended, and we demonstrated that the areas that are poorly modeled are localized and do not affect the accuracy of the prediction of other parts of the molecule. This further strengthens the conclusion of additive behavior in the magnetic response of polycyclic aromatic systems.

In the course of these analyses, we investigated the role of topology in the molecular bond-currents. We showed that the shape itself of the molecule (i.e., analogous to a wire loop in various shapes) has a minimal effect on the bond-currents, even though the annulation types themselves are the deciding factor. The uniform-current model we applied to study this highlighted the importance of the currents located on the fused bonds and of the variance in circumference current strength, and supported the design of the additivity methods we constructed.

The BAdd method we implemented for the purposes of this study is, to the best of our knowledge, the first "bottom-up" additivity method based on BCSs. In contrast with previous methods, it uses a small, fixed-size library of building blocks that are universally applicable to all unbranched *cata*-condensed PBHs. The quantitative results the method affords allow for comparison of BCSs and NICS values within a single molecule, as well as comparison between different molecules. Therefore, we believe the BAdd and the NAdd can potentially become widely-used tools for the characterization of PASs. We emphasize that poorly-modeled substructures do not harm prediction in other areas of the molecule, and that even in such areas the maximum error appears to stay in a well-defined and constant margin, regardless of the length of the molecule. This allows for clear demarcation of the limitations and possible deviations of the methods, which is key to having confidence in them. Moreover, we believe these clear guidelines are necessary for making informed and reliable interpretations based on the results. In our view, the methods mostly succeed in reproducing explicitly-calculated values, with results varying from satisfactory to excellent. Nevertheless, with the knowledge gained in this study, we have identified possible avenues to further improve the accuracy, which we will explore in the near future.

Acknowledgements

The authors wish to express their thanks to Alexandra Wahab for her assistance with Predi-XY, to Dr. Alexandra Tsybizova for proofreading the manuscript, to Prof. Dr. Peter Chen for his ongoing financial and scientific support, and to Dr. Riccardo Zanasi for providing us with a copy of SYSMOIC and for his assistance with running the program. All authors thank the ETH Zürich, and R.G.P. acknowledges the financial support of The Branco Weiss Fellowship.

Data availability

The data that supports the findings of this study are available within the article [and its supplementary material]. The code used to implement the procedures described in this report is available from the corresponding author upon request and will also be included in the next release of Predi-XY,[34] which is freely downloadable from our group's GitLab repository.

Supporting Information

The following data are available in the Supporting Information: geometries for all structures considered in this study; BC^{ref}, BC^{BAdd}, $NICS^{ref}$, $NICS^{BC}$, $NICS^{BAdd}$, and $NICS^{NAdd}$ results for all compounds; NICS-XY-Scans from the uniform-current model for all compounds; MUEs and maximal errors for all compounds.

Appendix A: Short overview of the NICS method

The Nucleus-Independent Chemical Shift (NICS) method belongs to the magnetic criterion of aromaticity, which stems from the Ring-Current Model (RCM).[16–21] When a molecule is placed into an external magnetic field, currents are induced by the interaction of the molecule's electrons with the field. The RCM refers to the specific case when an aromatic ring is placed into an external magnetic field that is perpendicular to the molecular plane, and an induced current is formed by the cyclic motion of the π-electrons around the conjugated ring, i.e., the ring-current. As a result of the induced current, an induced magnetic field is generated in the aromatic molecule such that, in the center of the ring, it is opposite (antiparallel) to the external magnetic field, and outside the ring, it is parallel to the external field. For antiaromatic molecules, the induced ring-current has the opposite direction, leading to an opposite direction of the induced magnetic field. The strength of the induced magnetic field is an indication of the strength of the induced ring-current, which is assumed to be in direct correlation to the extent of aromaticity of the molecule.[86] Its strength can be assessed experimentally, e.g., with NMR,[91] or with computational approaches. One of the advantages of computational approaches is that they allow one to sample the induced field strength at any point. Indeed, that is what the NICS method does: the NICS "probe" is essentially a point in space for which the calculation of the chemical shielding tensor is requested. By convention, the probe is generally placed at or

above the ring center and the negative of the chemical shielding is reported; negative (positive) values indicate diatropic (paratropic) ring-currents, which usually imply aromatic (antiaromatic) behavior. For PASs, a NICS-based method is often used, termed the NICS-XY-Scan,[26] whereby a series of NICS probes is placed along a pathway that traverses the molecule. When the individual NICS values are plotted against the distance, a shape emerges, which can be interpreted in terms of local trends in the ring-currents of the molecule. For example, a single molecule may contain areas characterized by stronger/weaker currents, or even currents of opposing sense (which can sometimes mean aromatic and antiaromatic character residing side by side).[92,36] Importantly, the NICS-XY-Scan can be used with different types of NICS metrics, including the most refined version, $NICS(r)_{\pi ZZ}$, which has been shown to be the NICS-based metric closest to what we think aromaticity is[93] and the one that agrees best with ring-current analysis.[94]

References

[1] J.E. Anthony, Chem. Rev. **106**, 5028 (2006).
[2] C. Aumaitre and J.-F. Morin, Chem. Rec. **19**, 1142 (2019).
[3] P.M. Grant and I.P. Batra, Synth. Met. **1**, 193 (1980).
[4] A. Jurić, N. Trinajstić, and G. Jashari, Croat. Chem. Acta **59**, 617 (1986).
[5] L. Loots and L. J. Barbour, CrystEngComm **14**, 300 (2012).
[6] C. Sutton, C. Risko, and J.-L. Brédas, Chem. Mater. **28**, 3 (2016).
[7] J.E. Campbell, J. Yang, and G.M. Day, J. Mater. Chem. C **5**, 7574 (2017).
[8] A. Thiessen, H. Wettach, K. Meerholz, F. Neese, S. Höger, and D. Hertel, Org. Electron. **13**, 71 (2012).
[9] J.-H. Dou, Y.-Q. Zheng, Z.-F. Yao, Z.-A. Yu, T. Lei, X. Shen, X.-Y. Luo, J. Sun, S.-D. Zhang, Y.-F. Ding, G. Han, Y. Yi, J.-Y. Wang, and J. Pei, J. Am. Chem. Soc. **137**, 15947 (2015).
[10] Y. Wang, B. Liu, C.W. Koh, X. Zhou, H. Sun, J. Yu, K. Yang, H. Wang, Q. Liao, H.Y. Woo, and X. Guo, Adv. Energy Mater. **9**, 1803976 (2019).
[11] A. Kovalenko, C. Yumusak, P. Heinrichova, S. Stritesky, L. Fekete, M. Vala, M. Weiter, N.S. Sariciftci, and J. Krajcovic, J. Mater. Chem. C **5**, 4716 (2017).
[12] J. Lee, S.A. Park, S.U. Ryu, D. Chung, T. Park, and S.Y. Son, J. Mater. Chem. A **8**, 21455 (2020).
[13] C. Di, G. Yu, Y. Liu, and D. Zhu, J. Phys. Chem. B **111**, 14083 (2007).
[14] X. He, L. Yin, and Y. Li, J. Mater. Chem. C **7**, 2487 (2019).
[15] V.V. Brus, J. Lee, B.R. Luginbuhl, S.-J. Ko, G.C. Bazan, and T.-Q. Nguyen, Adv. Mater. **31**, 1900904 (2019).
[16] L. Pauling, J. Chem. Phys. **4**, 673 (1936).
[17] K.Y. Lonsdale and W.H. Bragg, Proc. R. Soc. Lond. Ser. - Math. Phys. Sci. **159**, 149 (1937).
[18] F. London, J Phys Radium **8**, 397 (1937).
[19] J.A. Pople, Mol Phys **1**, 175 (1958).
[20] R. McWeeny, Mol. Phys. **1**, 311 (1958).
[21] T.K. Dickens and R.B. Mallion, MATCH Commun. Math. Comput. Chem. **76**, 297 (2016).
[22] M. Bilde and A.E. Hansen, Mol. Phys. **92**, 237 (1997).
[23] P. v R. Schleyer, C. Maerker, A. Dransfeld, H. Jiao, and N.J.R. van Eikema Hommes, J. Am. Chem. Soc. **118**, 6317 (1996).
[24] Z. Chen, C.S. Wannere, C. Corminboeuf, R. Puchta, and P. von R. Schleyer, Chem. Rev. **105**, 3842 (2005).
[25] R. Gershoni-Poranne and A. Stanger, Chem. Soc. Rev. **44**, 6597 (2015).
[26] R. Gershoni-Poranne and A. Stanger, Chem. – Eur. J. **20**, 5673 (2014).
[27] J.J. Dressler and M.M. Haley, J. Phys. Org. Chem. **33**, e4114 (2020).
[28] C.K. Frederickson, L.N. Zakharov, and M.M. Haley, J. Am. Chem. Soc. **138**, 16827 (2016).
[29] J. Cao, G. London, O. Dumele, M. von Wantoch Rekowski, N. Trapp, L. Ruhlmann, C. Boudon, A. Stanger, and F. Diederich, J. Am. Chem. Soc. **137**, 7178 (2015).
[30] J.V. Milić, C. Schaack, N. Hellou, F. Isenrich, R. Gershoni-Poranne, D. Neshchadin, S. Egloff, N. Trapp, L. Ruhlmann, C. Boudon, G. Gescheidt, J. Crassous, and F. Diederich, J. Phys. Chem. C **122**, 19100 (2018).
[31] R. Gershoni-Poranne, A.P. Rahalkar, and A. Stanger, Phys. Chem. Chem. Phys. **20**, 14808 (2018).
[32] R. Gershoni-Poranne, Chem. – Eur. J. **24**, 4165 (2018).
[33] P. Finkelstein and R. Gershoni-Poranne, ChemPhysChem **20**, 1508 (2019).

[34] A. Wahab, F. Fleckenstein, S. Feusi, and R. Gershoni-Poranne, Electron. Struct. (2020).
[35] S. Van Damme, G. Acke, R.W.A. Havenith, and P. Bultinck, Phys. Chem. Chem. Phys. **18**, 11746 (2016).
[36] A. Stanger, G. Monaco, and R. Zanasi, ChemPhysChem **21**, 65 (2020).
[37] P.W. Fowler, S. Cotton, D. Jenkinson, W. Myrvold, and W.H. Bird, Chem. Phys. Lett. **597**, 30 (2014).
[38] M.J. Frisch, G.W. Trucks, H.B. Schlegel, G.E. Scuseria, M.A. Robb, J.R. Cheeseman, G. Scalmani, V. Barone, B. Mennucci, G.A. Petersson, H. Nakatsuji, M. Caricato, X. Li, H.P. Hratchian, A.F. Izmaylov, J. Bloino, G. Zheng, J.L. Sonnenberg, M. Hada, M. Ehara, K. Toyota, R. Fukuda, J. Hasegawa, M. Ishida, T. Nakajima, Y. Honda, O. Kitao, H. Nakai, T. Vreven, J.A. Montgomery, Jr., J.E. Peralta, F. Ogliaro, M. Bearpark, J.J. Heyd, E. Brothers, K.N. Kudin, V.N. Staroverov, R. Kobayashi, J. Normand, K. Raghavachari, A. Rendell, J.C. Burant, S.S. Iyengar, J. Tomasi, M. Cossi, N. Rega, J.M. Millam, M. Klene, J.E. Knox, J.B. Cross, V. Bakken, C. Adamo, J. Jaramillo, R. Gomperts, R.E. Stratmann, O. Yazyev, A.J. Austin, R. Cammi, C. Pomelli, J.W. Ochterski, R.L. Martin, K. Morokuma, V.G. Zakrzewski, G.A. Voth, P. Salvador, J.J. Dannenberg, S. Dapprich, A.D. Daniels, Ö. Farkas, J.B. Foresman, J.V. Ortiz, J. Cioslowski, and D.J. Fox, *Gaussian09 Revision D.01* (Gaussian, Inc., Wallingford CT, 2009).
[39] C. Lee, W. Yang, and R.G. Parr, Phys. Rev. B **37**, 785 (1988).
[40] A.D. Becke, J. Chem. Phys. **98**, 5648 (1993).
[41] J.S. Binkley, J.A. Pople, and W.J. Hehre, J. Am. Chem. Soc. **102**, 939 (1980).
[42] M.J. Frisch, J.A. Pople, and J.S. Binkley, J. Chem. Phys. **80**, 3265 (1984).
[43] S. Grimme, J. Antony, S. Ehrlich, and H. Krieg, J. Chem. Phys. **132**, 154104 (2010).
[44] R. Ditchfield, Mol. Phys. **27**, 789 (1974).
[45] G. Schreckenbach and T. Ziegler, J. Phys. Chem. **99**, 606 (1995).
[46] A. Stanger, J. Org. Chem. **71**, 883 (2006).
[47] A. Stanger, J. Org. Chem. **75**, 2281 (2010).
[48] A.P. Rahalkar and A. Stanger, *Aroma* (Http://Schulich.Technion.Ac.Il/Amnon_stanger.Htm 2014, n.d.).
[49] J.A. Bohmann, F. Weinhold, and T.C. Farrar, J. Chem. Phys. **107**, 1173 (1997).
[50] E.D. Glendening, C.R. Landis, and F. Weinhold, WIREs Comput. Mol. Sci. **2**, 1 (2012).
[51] T.A. Keith and R.F.W. Bader, Chem. Phys. Lett. **210**, 223 (1993).
[52] G. Monaco, F.F. Summa, and R. Zanasi, *SYSMOIC a Package for the Calculation of the Magnetically Induced Current Density in Molecular Systems* (University of Salerno, 2019).
[53] J. Jusélius, D. Sundholm, and J. Gauss, J. Chem. Phys. **121**, 3952 (2004).
[54] T.J.P. Irons, L. Spence, G. David, B.T. Speake, T. Helgaker, and A.M. Teale, J. Phys. Chem. A (2020).
[55] P.J. Davis and P. Rabinowitz, in *Methods Numer. Integr. Second Ed.*, edited by P.J. Davis and P. Rabinowitz (Academic Press, 1984), pp. 51–198.
[56] B. Cordero, V. Gómez, A.E. Platero-Prats, M. Revés, J. Echeverría, E. Cremades, F. Barragán, and S. Alvarez, Dalton Trans. 2832 (2008).
[57] H. Fliegl, S. Taubert, O. Lehtonen, and D. Sundholm, Phys. Chem. Chem. Phys. **13**, 20500 (2011).
[58] J.D. Jackson, *Classical Electrodynamics* (John Wiley & Sons, Inc., 1998).
[59] H.C. Longuet-Higgins and L. Salem, Proc. R. Soc. Lond. Ser. Math. Phys. Sci. **257**, 445 (1960).
[60] R.B. Mallion, Mol. Phys. **25**, 1415 (1973).
[61] G. Monaco, R. Zanasi, S. Pelloni, and P. Lazzeretti, J. Chem. Theory Comput. **6**, 3343 (2010).

[62] R.P. Brent, Comput. J. **14**, 422 (1971).
[63] C.R. Harris, K.J. Millman, S.J. van der Walt, R. Gommers, P. Virtanen, D. Cournapeau, E. Wieser, J. Taylor, S. Berg, N.J. Smith, R. Kern, M. Picus, S. Hoyer, M.H. van Kerkwijk, M. Brett, A. Haldane, J.F. del Río, M. Wiebe, P. Peterson, P. Gérard-Marchant, K. Sheppard, T. Reddy, W. Weckesser, H. Abbasi, C. Gohlke, and T.E. Oliphant, Nature **585**, 357 (2020).
[64] P. Virtanen, R. Gommers, T.E. Oliphant, M. Haberland, T. Reddy, D. Cournapeau, E. Burovski, P. Peterson, W. Weckesser, J. Bright, S.J. van der Walt, M. Brett, J. Wilson, K.J. Millman, N. Mayorov, A.R.J. Nelson, E. Jones, R. Kern, E. Larson, C.J. Carey, İ. Polat, Y. Feng, E.W. Moore, J. VanderPlas, D. Laxalde, J. Perktold, R. Cimrman, I. Henriksen, E.A. Quintero, C.R. Harris, A.M. Archibald, A.H. Ribeiro, F. Pedregosa, and P. van Mulbregt, Nat. Methods **17**, 261 (2020).
[65] A.A. Hagberg, D.A. Schult, and P.J. Swart, in *Proc. 7th Python Sci. Conf.* (2008), pp. 11–15.
[66]*The PyMOL Molecular Graphics System* (Schrödinger, LLC., 2014).
[67] J.D. Hunter, Comput. Sci. Eng. **9**, 90 (2007).
[68] M. Randic, J. Am. Chem. Soc. **99**, 444 (1977).
[69] M. Randić, Tetrahedron **33**, 1905 (1977).
[70] M. Randić, Chem. Phys. Lett. **38**, 68 (1976).
[71] J.A.N.F. Gomes, Croat. Chem. Acta **53**, 561 (1980).
[72] M. Mandado, J. Chem. Theory Comput. **5**, 2694 (2009).
[73] J. Aihara, J. Phys. Org. Chem. **21**, 79 (2008).
[74] J. Aihara, J. Am. Chem. Soc. **128**, 2873 (2006).
[75] M.O. Hamzah, M.S. Hadi, S.H. Saleh, I.M.M. Hassan, S.F. Nareen, and I.A. Hussen, AIP Conf. Proc. **2213**, 020009 (2020).
[76] S. Fias, P.W. Fowler, J.L. Delgado, U. Hahn, and P. Bultinck, Chem. – Eur. J. **14**, 3093 (2008).
[77] G. Monaco and R. Zanasi, J. Chem. Phys. **131**, 044126 (2009).
[78] R. Zanasi, P.D. Porta, and G. Monaco, J. Phys. Org. Chem. **29**, 793 (2016).
[79] T.K. Dickens and R.B. Mallion, Phys. Chem. Chem. Phys. **15**, 8245 (2013).
[80] T.K. Dickens and R.B. Mallion, J. Phys. Chem. A **122**, 7666 (2018).
[81] T.K. Dickens and R.B. Mallion, J. Phys. Chem. A **124**, 7973 (2020).
[82] G. Monaco, M. Memoli, and R. Zanasi, J. Phys. Org. Chem. **26**, 109 (2013).
[83] T.K. Dickens and R.B. Mallion, J. Phys. Chem. A **118**, 3688 (2014).
[84] S. Pelloni, G. Monaco, P. Lazzeretti, and R. Zanasi, Phys. Chem. Chem. Phys. **13**, 20666 (2011).
[85] G. Monaco and R. Zanasi, Phys. Chem. Chem. Phys. **18**, 11800 (2016).
[86] J.A.N.F. Gomes and R.B. Mallion, Chem. Rev. **101**, 1349 (2001).
[87] T.K. Dickens, J.A.N.F. Gomes, and R.B. Mallion, J. Chem. Theory Comput. **7**, 3661 (2011).
[88] D. W. Szczepanik, M. Solà, T. M. Krygowski, H. Szatylowicz, M. Andrzejak, B. Pawełek, J. Dominikowska, M. Kukułka, and K. Dyduch, Phys. Chem. Chem. Phys. **20**, 13430 (2018).
[89] Y. Yang, E.R. Davidson, and W. Yang, Proc. Natl. Acad. Sci. **113**, E5098 (2016).
[90] H. Okamoto, S. Hamao, R. Eguchi, H. Goto, Y. Takabayashi, P.Y.-H. Yen, L.U. Liang, C.-W. Chou, G. Hoffmann, S. Gohda, H. Sugino, Y.-F. Liao, H. Ishii, and Y. Kubozono, Sci. Rep. **9**, (2019).
[91] R.H. Mitchell, Chem. Rev. **101**, 1301 (2001).
[92] R. Gershoni-Poranne, C.M. Gibson, P.W. Fowler, and A. Stanger, J. Org. Chem. **78**, 7544 (2013).
[93] H. Fallah-Bagher-Shaidaei, C.S. Wannere, C. Corminboeuf, R. Puchta, and P. v R. Schleyer, Org. Lett. **8**, 863 (2006).
[94] R. Báez-Grez, L. Ruiz, R. Pino-Rios, and W. Tiznado, RSC Adv. **8**, 13446 (2018).

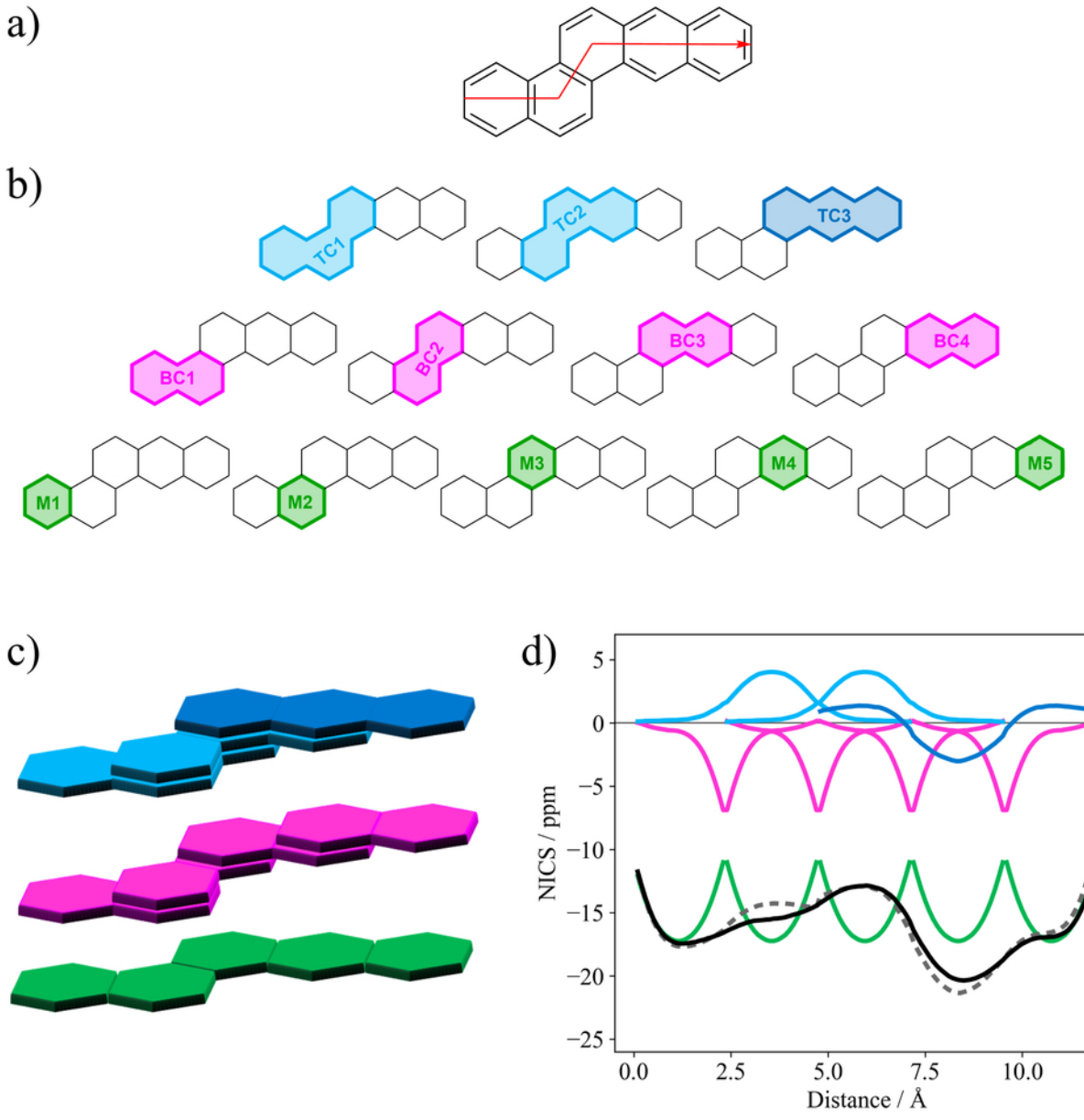
a)
b)
TC1
TC2
TC3
BC1
BC2
BC3
BC4
M1
M2
M3
M4
M5
c)
d)
NICS / ppm
Distance / Å
5
0
−5
−10
−15
−20
−25
0.0
2.5
5.0
7.5
10.0

a)

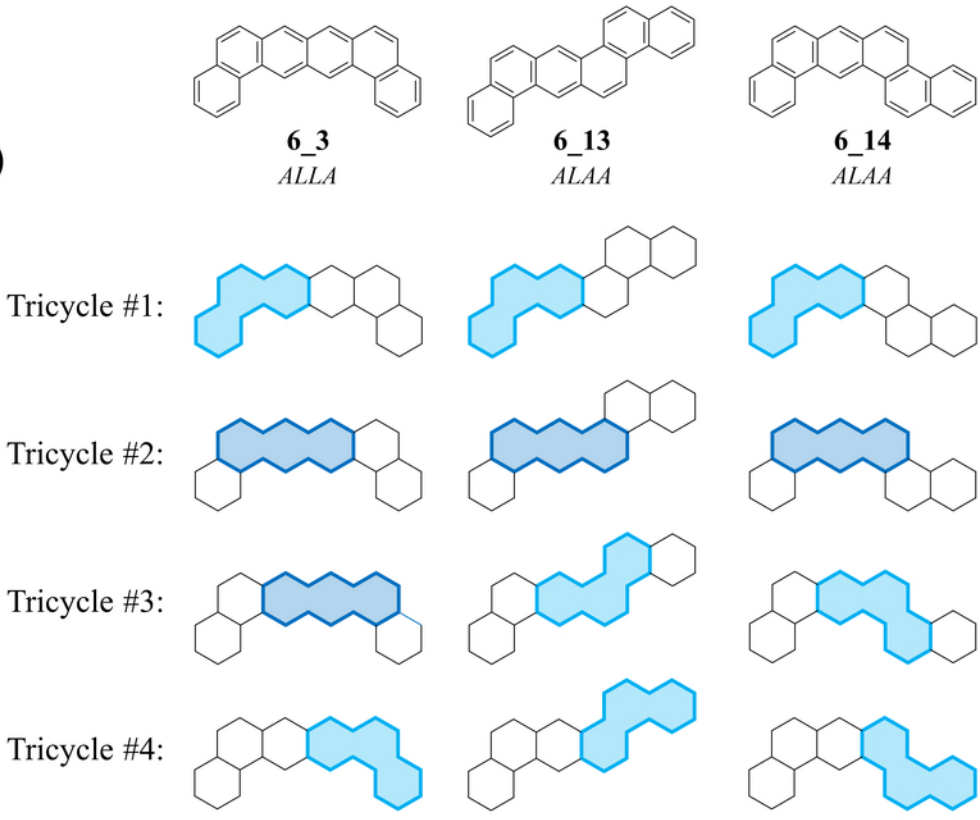
6_3
ALLA
6_13
ALAA
6_14
ALAA
Tricycle #1:
Tricycle #2:
Tricycle #3:
Tricycle #4:

b)

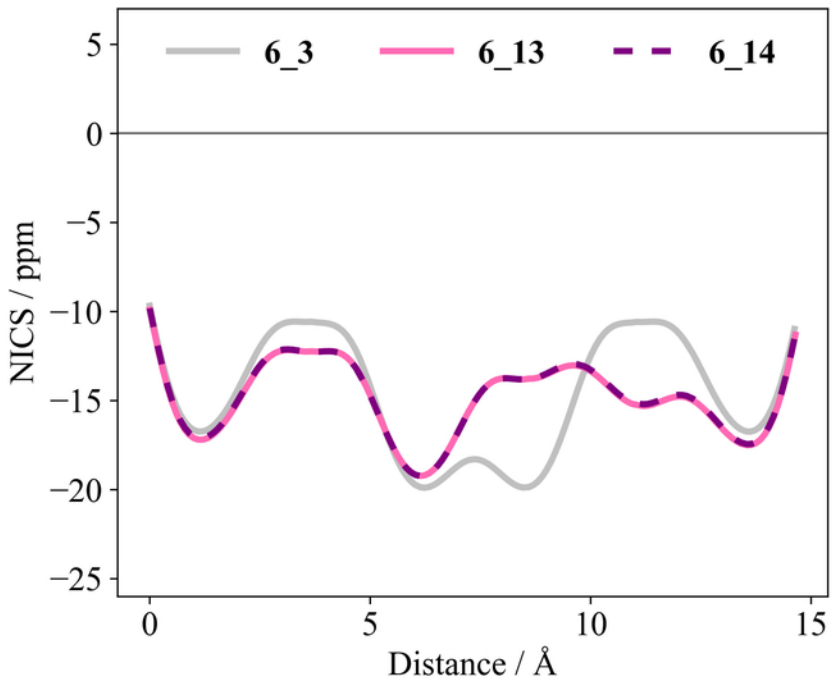
6_3
6_13
6_14
5
0
−5
−10
−15
−20
−25
NICS / ppm
0
5
10
15
Distance / Å

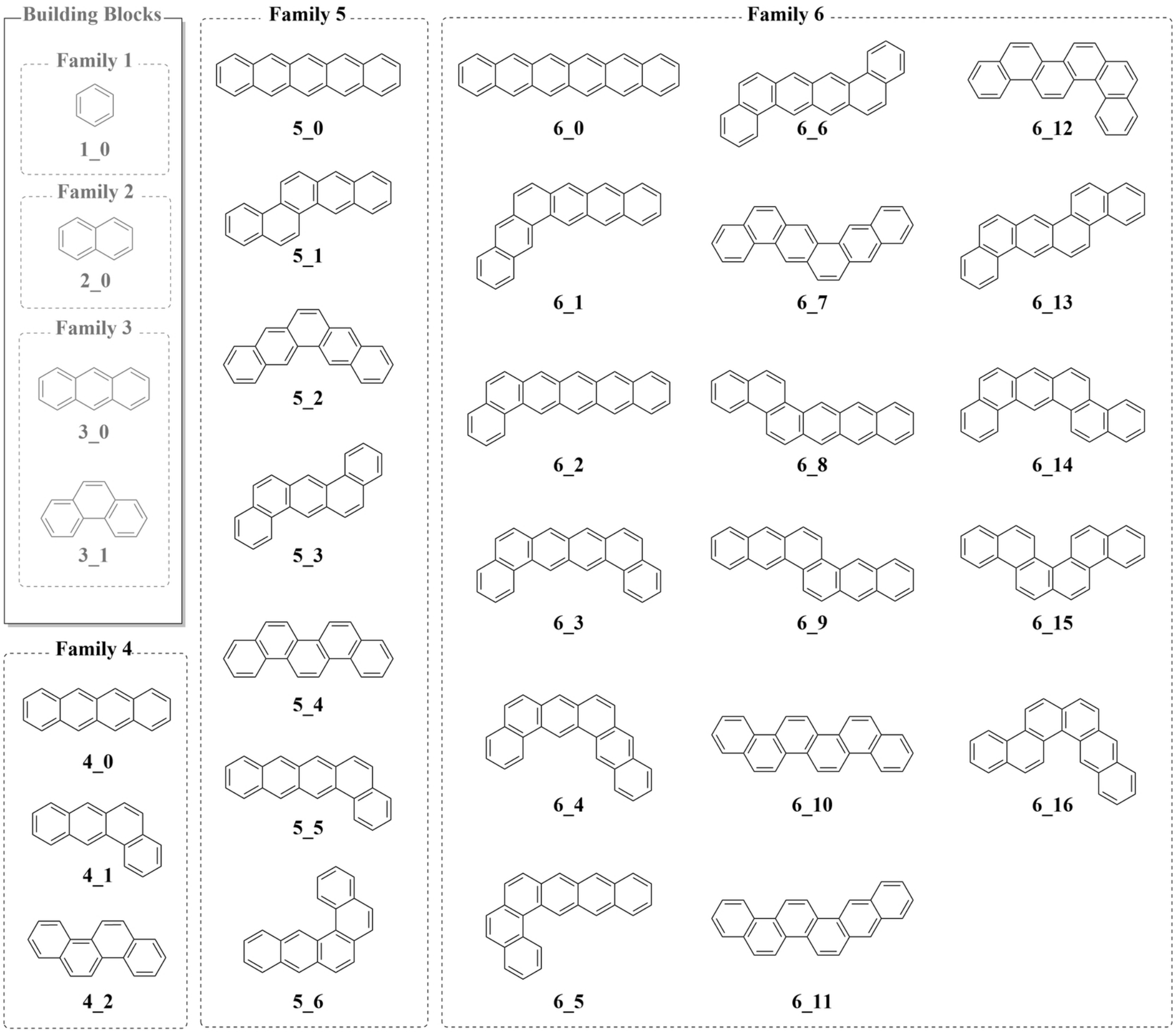
Building Blocks
Family 1
1_0
Family 2
2_0
Family 3
3_0
3_1
Family 4
4_0
4_1
4_2
Family 5
5_0
5_1
5_2
5_3
5_4
5_5
5_6
Family 6
6_0
6_6
6_12
6_1
6_7
6_13
6_2
6_8
6_14
6_3
6_9
6_15
6_4
6_10
6_16
6_5
6_11

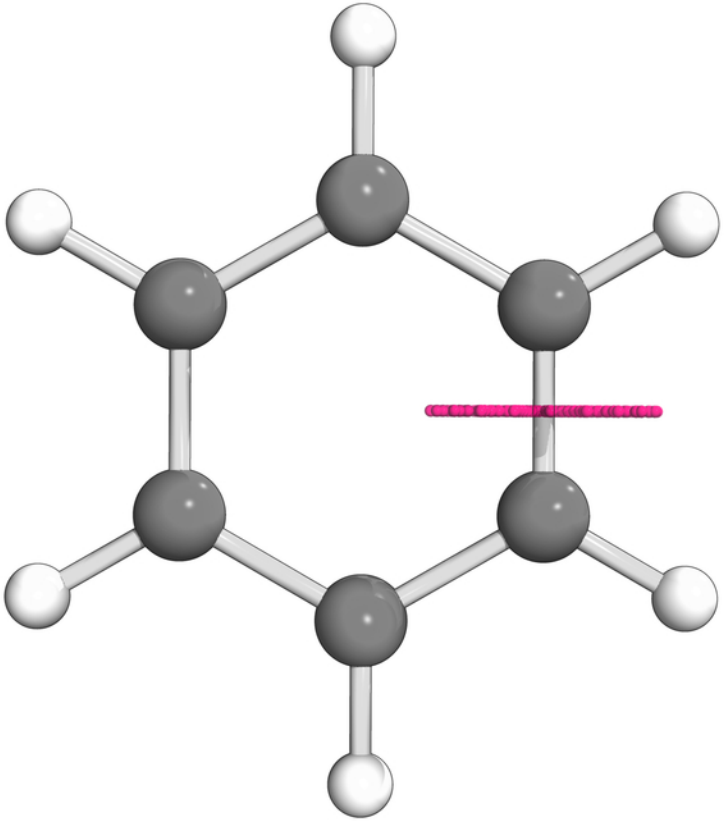

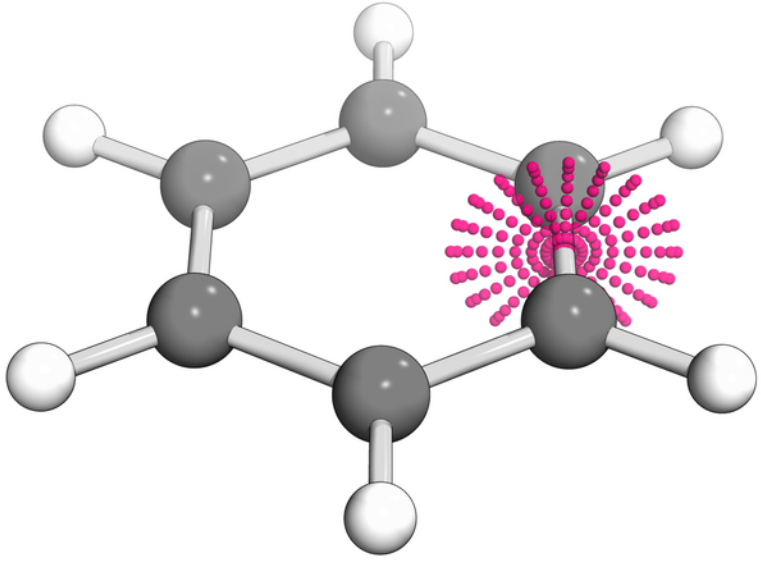

a)

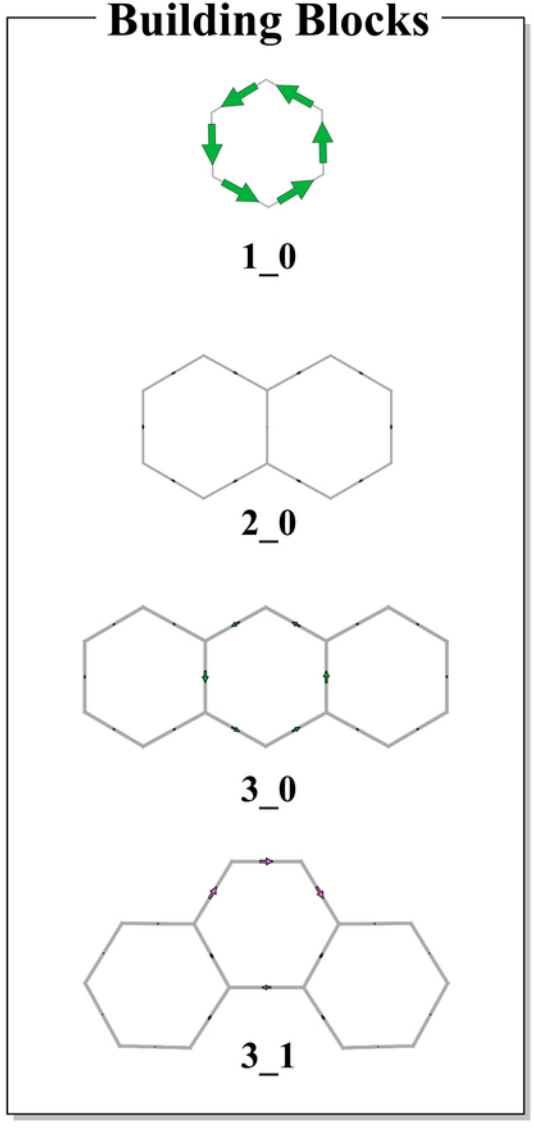
Building Blocks
1_0
2_0
3_0
3_1

b)

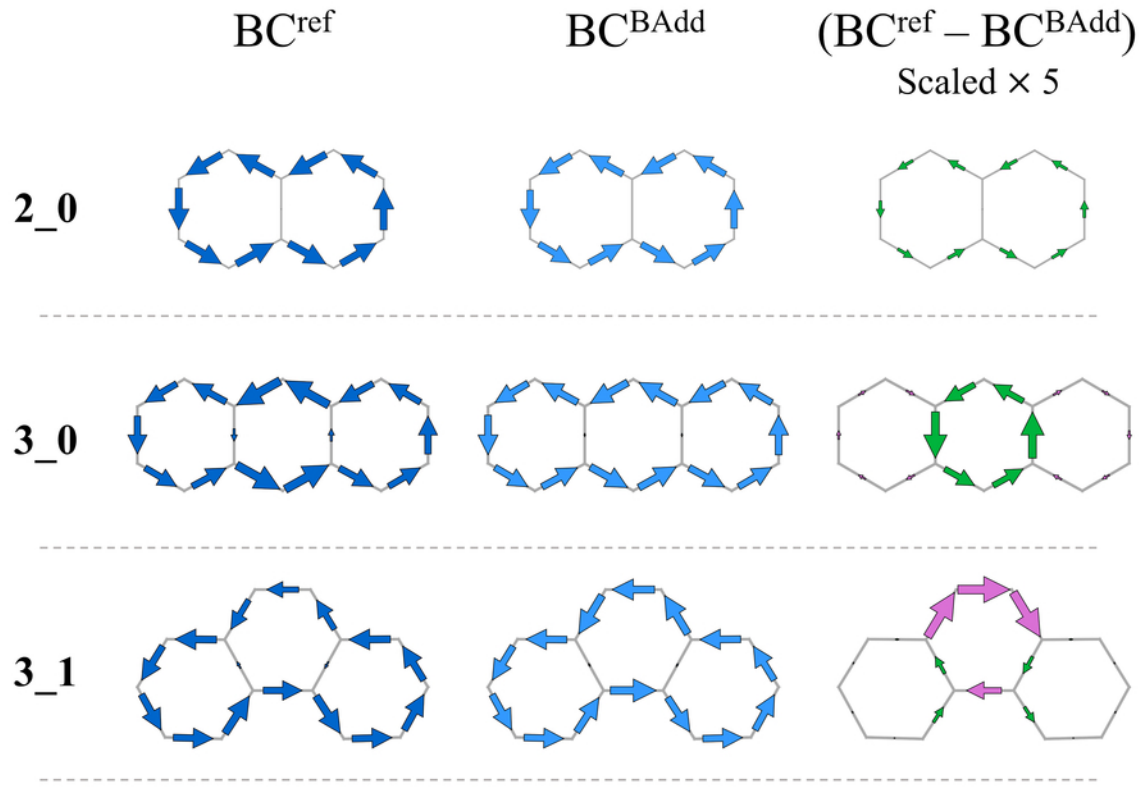
BC^ref
BC^BAdd
(BC^ref – BC^BAdd)
Scaled × 5
2_0
3_0
3_1

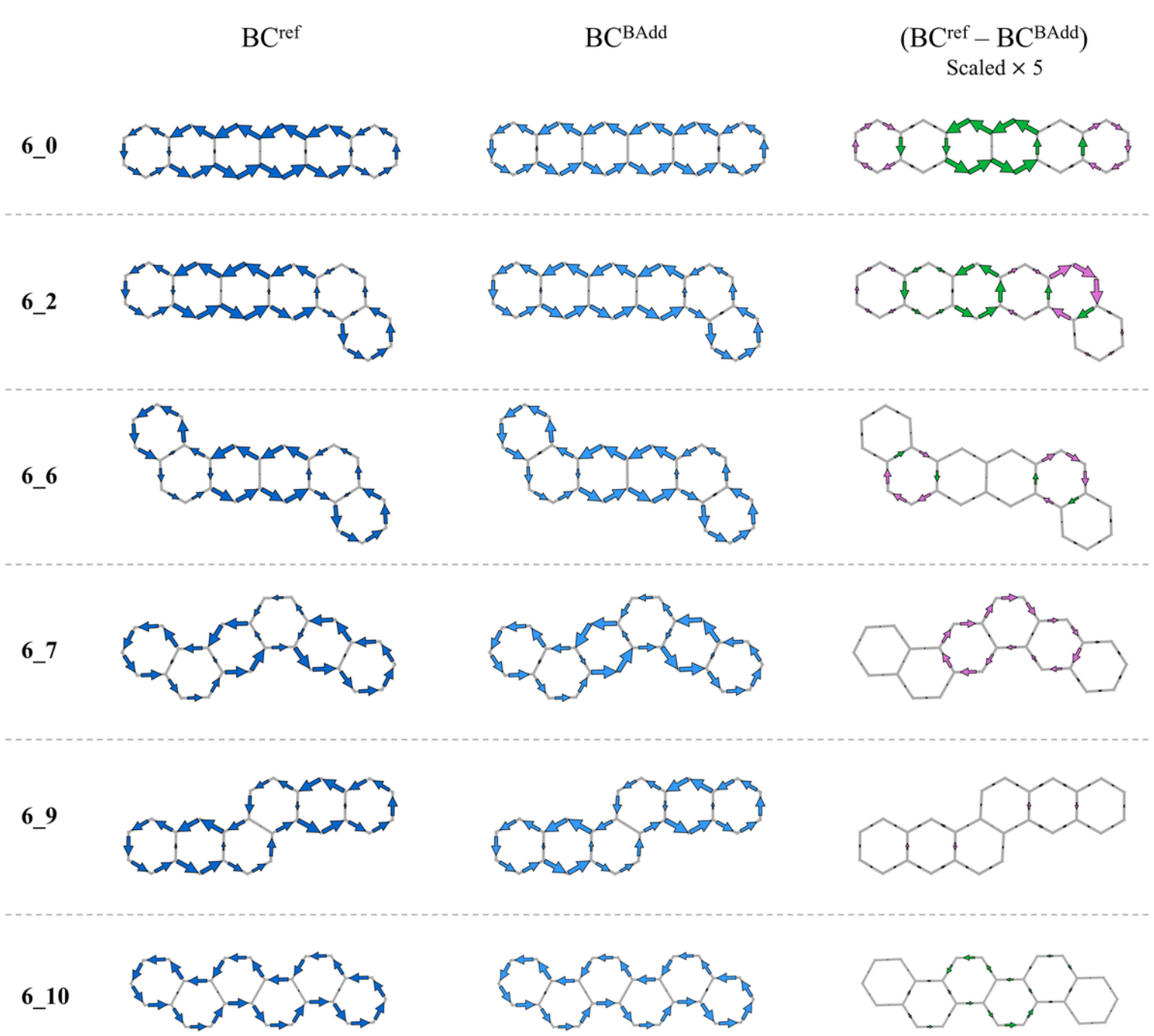
BC^ref
BC^BAdd
(BC^ref – BC^BAdd)
Scaled × 5
6_0
6_2
6_6
6_7
6_9
6_10

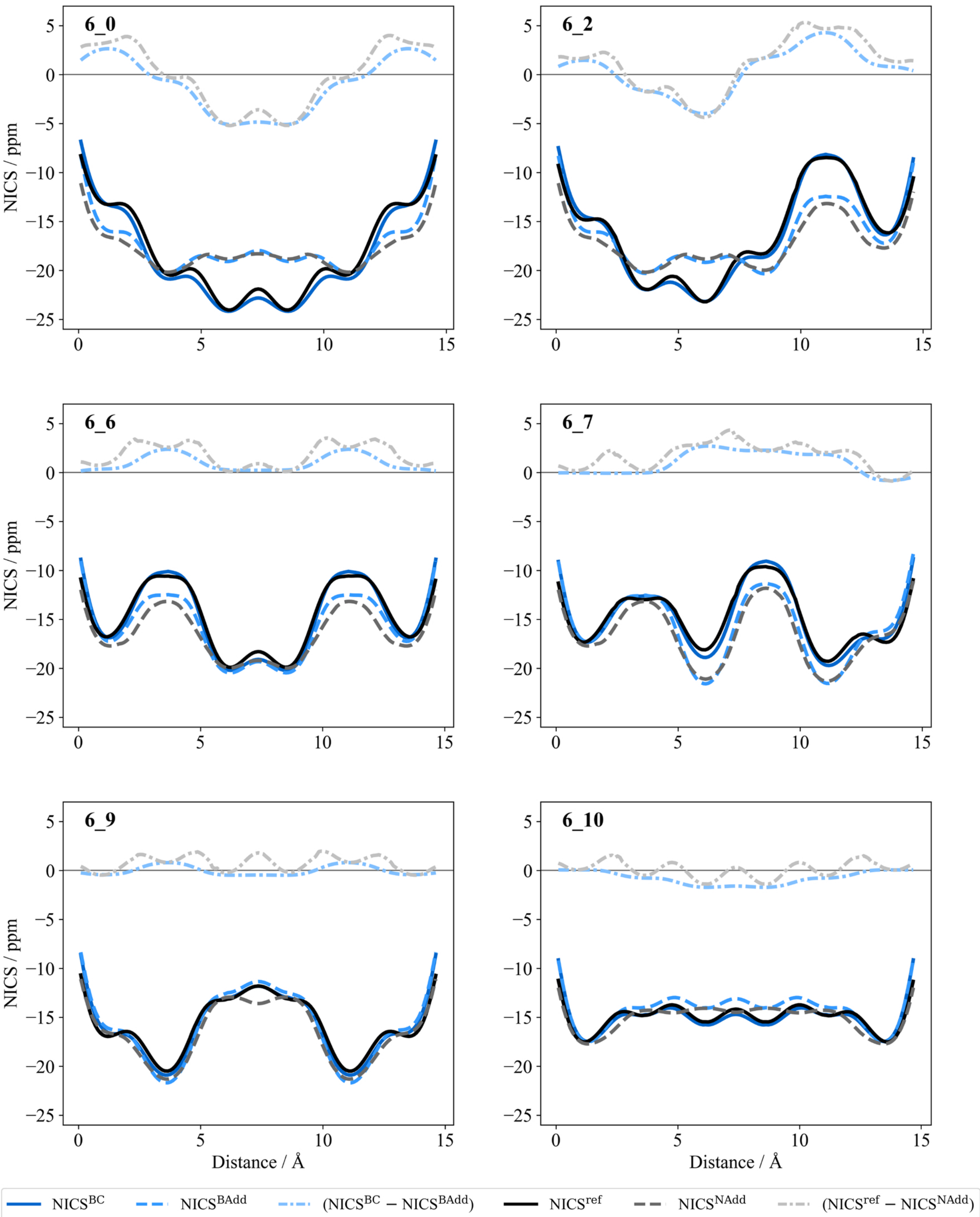
6_0
6_2
6_6
6_7
6_9
6_10
NICS / ppm
Distance / Å
NICS^BC
NICS^BAdd
(NICS^BC − NICS^BAdd)
NICS^ref
NICS^NAdd
(NICS^ref − NICS^NAdd)

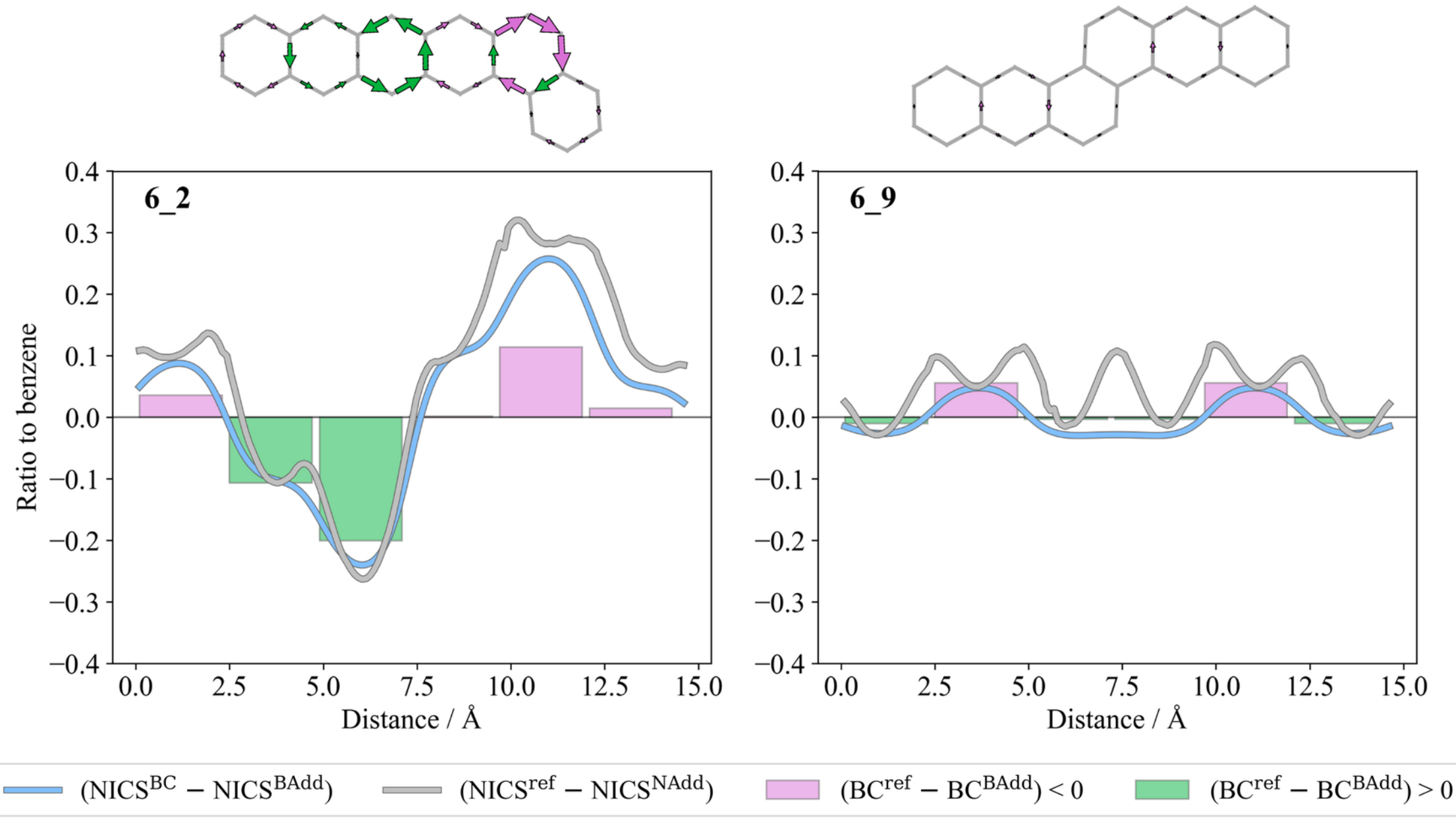
6_2
6_9
Ratio to benzene
Distance / Å
Distance / Å
0.4
0.3
0.2
0.1
0.0
−0.1
−0.2
−0.3
−0.4
0.0
2.5
5.0
7.5
10.0
12.5
15.0
(NICS^BC − NICS^BAdd)
(NICS^ref − NICS^NAdd)
(BC^ref − BC^BAdd) < 0
(BC^ref − BC^BAdd) > 0

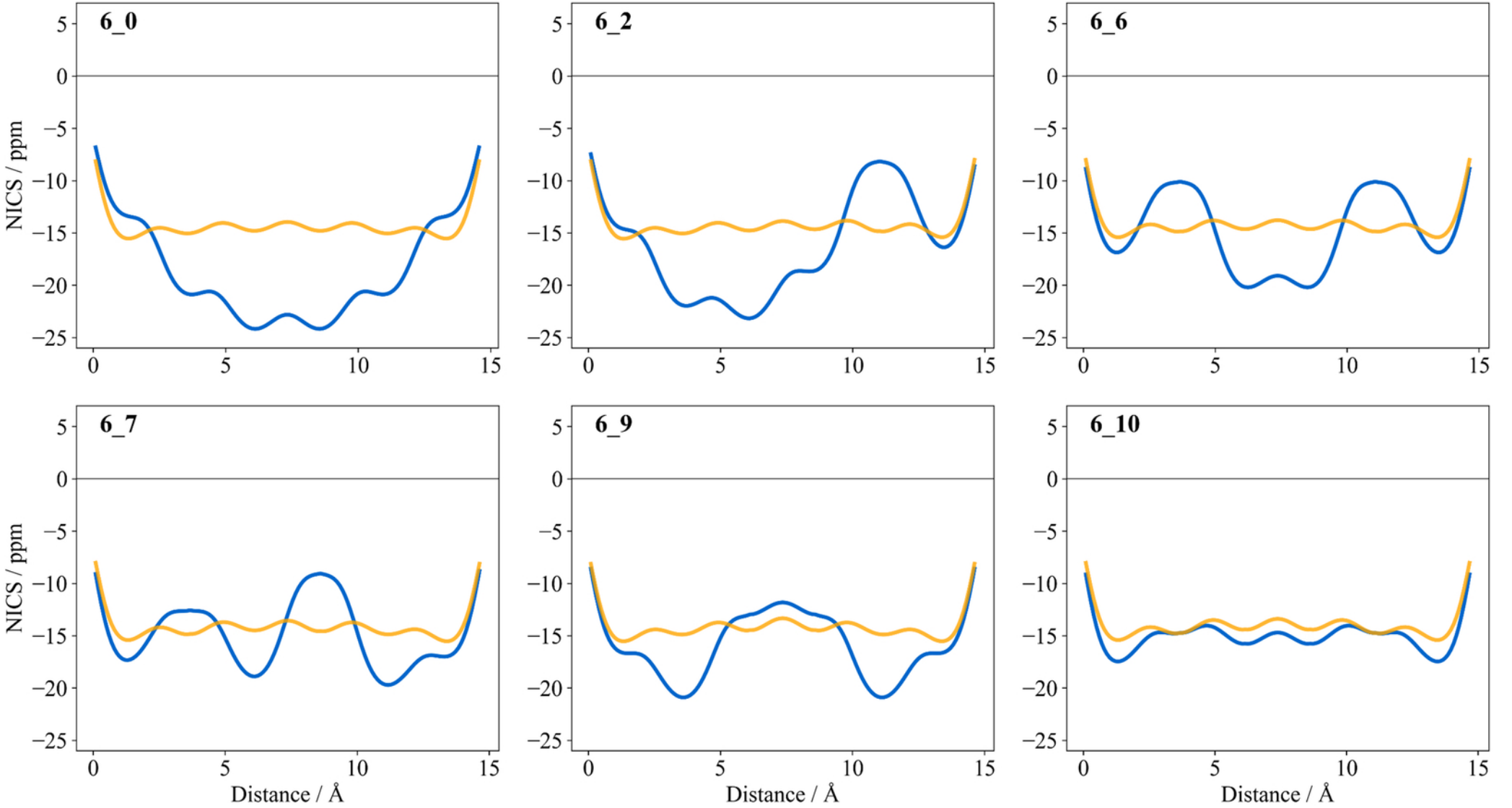
6_0
6_2
6_6
6_7
6_9
6_10
NICS / ppm
Distance / Å
5
0
−5
−10
−15
−20
−25
0
5
10
15

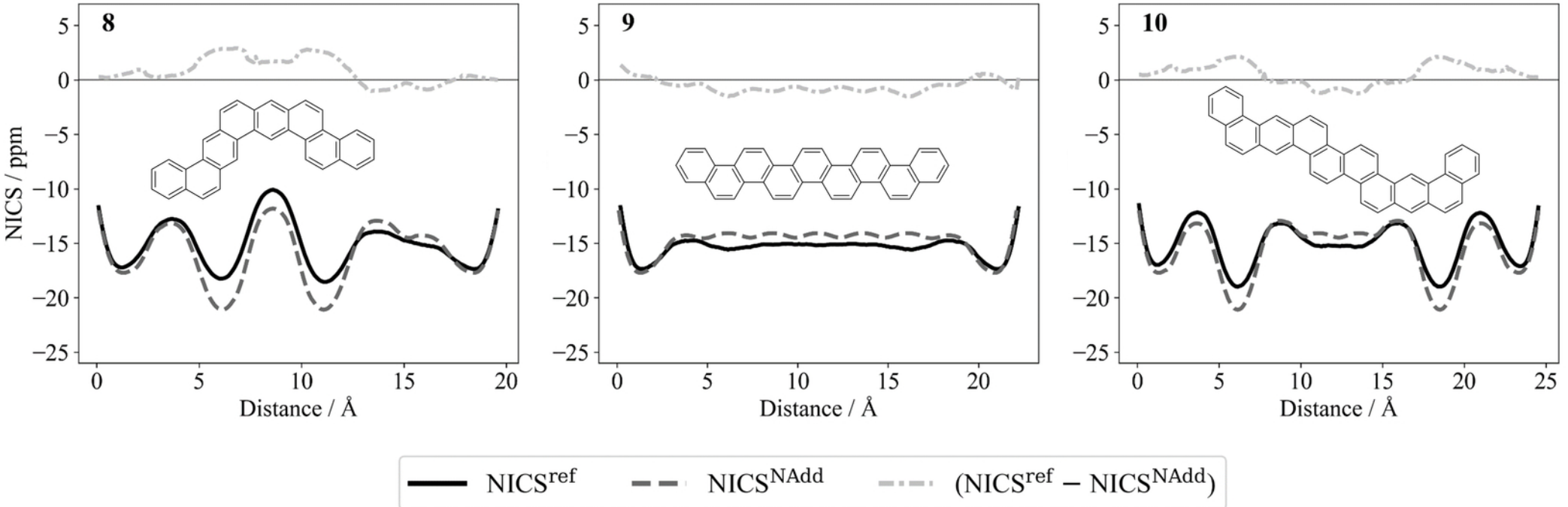
8
9
10
NICS / ppm
Distance / Å
Distance / Å
Distance / Å
NICS^ref
NICS^NAdd
(NICS^ref − NICS^NAdd)